Ocean Engineering 316 (2025) 120000

Contents lists available at ScienceDirect

Ocean Engineering

journal homepage: www.elsevier.com/locate/oceaneng

Research paper

The effect of installation advancement ratio on interaction between helices of screw piles for offshore renewable energy

Wei Wang [a,*], Michael John Brown [a], Matteo Oryem Ciantia [a,b], Marco Previtali [a], Yaseen Umar Sharif [a], Craig Davidson [a]

[a] School of Science and Engineering, University of Dundee, Fulton Building, Dundee, DD1 4HN, UK
[b] Department of Earth and Environmental Sciences (DISAT), University Milano Bicocca, Italy

ARTICLE INFO

Keywords:
Discrete element modelling (DEM)
Screw pile
Helical anchor
Installation effect
Sand

ABSTRACT

Upscaled screw piles have been proposed as a novel silent foundation solution for both offshore jacket structures and anchoring in various renewable energy applications. Replacing conventional pitch-matched installation approaches by over-flighted installation approaches has been proposed for single-helix screw piles to reduce installation vertical crowd force and torque whilst enhancing in-service tensile capacity and stiffness. This study, using DEM modelling, extends the scope of investigation to consider multi-helix screw piles and investigates installation and tensile in-service response, addressing the effect of helix spacing and installation advancement ratio together. The findings suggest that a pile featuring smaller helix spacing may necessitate less vertical force and torque for installation than a single-helix pile if over-flighted installation approaches are used, although the first (bottom) helix needs to be 'deeply' embedded to avoid the reduction of tensile capacity induced by additional helices. This differs from piles installed by pitch-matched approaches where additional helices typically increase installation force and torque. DEM micromechanical analyses help unveil the mechanisms behind the macroscopic response of such screw piles.

1. Introduction

Screw piles have been widely used onshore for anchoring guy lines of e.g. transmission towers and small wind turbines (Cerato and Victor, 2014; Schiavon et al., 2019) and supporting residential and other structures e.g. traffic sign poles and solar panels (Feng et al., 2020; Perko, 2009). A screw pile typically consists of a straight shaft or core with one or more helices spaced at regular intervals up the core. Fig. 1 demonstrates typical geometrical properties of screw piles. L is the pile length, D_s and D_h are diameters of pile shaft and helix, respectively, p_h is helix geometric pitch, H_n is embedment depth of the nth helix from the pile base/tip, and S_h is the spacing between two adjacent helices. Conventionally onshore D_h ranges from 200 mm to 800 mm with D_s being up to 300 mm and with L being up to 10 m creating up to hundreds of kN of tensile capacity (Perko, 2009). To install onshore screw piles typically requires torque up to hundreds of kNm. A correlation factor K_t between finally installation torque (T) and pile tensile capacity (Q_t) is often used to verify installation or estimate capacity (British Standards Institution, 2015):

$$Q_t = K_t T \tag{1}$$

Recently screw piles have been suggested for use as an alternative silent foundation/anchoring solution for offshore renewable energy applications e.g. as foundations for jacket structures supporting wind turbines or as anchors for floating systems in deeper water (Al-Baghdadi, 2018; Cerfontaine et al., 2023c; Spagnoli and Tsuha, 2020). In contrast to onshore practice, the piles for the offshore applications may require upscaling to sizes where both D_h and D_s are measured in terms of meters and L is tens of meters, where the installation requires torque up to tens of MN (Cerfontaine et al., 2022; Davidson et al., 2022). Compared to conventional driven-in straight-shafted piles, the installation of screw piles, which involves rotation and pushing-in, is more environmentally friendly due to the reduced noise and vibration for marine animals (Herbert-Read et al., 2017). Also, it has a potential of easier decommissioning, by reverse rotation (Ding et al., 2019), and higher axial capacity if the same shaft diameter is adopted as in a straight-shafted

* Corresponding author. author.
E-mail addresses: 2422030@dundee.ac.uk (W. Wang), m.j.z.brown@dundee.ac.uk (M. John Brown), m.o.ciantia@dundee.ac.uk (M. Oryem Ciantia), m.z.previtali@dundee.ac.uk (M. Previtali), y.sharif@dundee.ac.uk (Y. Umar Sharif), c.s.davidson@dundee.ac.uk (C. Davidson).

https://doi.org/10.1016/j.oceaneng.2024.120000
Received 16 July 2024; Received in revised form 13 September 2024; Accepted 30 November 2024
Available online 6 December 2024

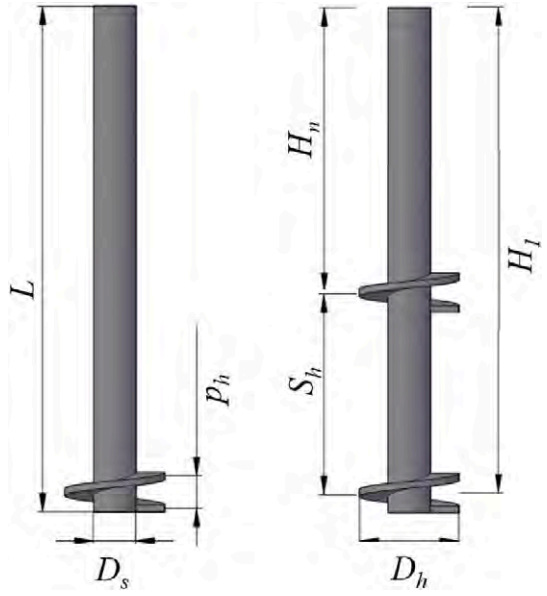

Fig. 1. Schematic diagram of screw piles and the typical terminology (left: single helix, right: dual helix).

pile (Al-Baghdadi, 2018).

Current standards e.g. BS8004 (British Standards Institution, 2015) recommend that a pitch-matched installation (advancement ratio, AR = 1.0, Bradshaw et al., 2019) should be employed with a tolerance of ± 0.15 to minimize the 'disturbance' of the in-situ soil. AR is defined as Eq. (2):

$$AR = \frac{2\pi v}{\omega p_h} \tag{2}$$

where v is the vertical penetration velocity, ω is the rotation rate, and p_h is the pitch of the helical plate. However, increasing the pile size for offshore applications has been shown to result in potentially prohibitive vertical (crowd) installation forces if the process follows the 'pitch-matched' approach (Davidson et al., 2022; Sharif et al., 2021a). One solution to reduce the large vertical installation forces is over-flighting (AR < 1.0) as this displaces soil upwards through the helix resulting in an increase and decrease of soil stress above and below the helix, respectively (Cerfontaine et al. 2021, 2023a; Sharif et al., 2021a). This soil stress variation also reduces the required torque during installation and improves post-installation monotonic tensile response at expense of monotonic compressive behaviour (Cerfontaine et al. 2019, 2021; Sharif et al., 2021a; Wang et al., 2023b). The improved tensile response is favourable for offshore applications where tensile behaviour may typically be more critical than the compressive requirements. However, the AR effects discussed above have only been observed for single-helix piles and not studied for piles with more than one helix.

Adopting a second helix may have the potential to increase uplift capacity due to greater bearing surface area although increased pile surface area is normally associated with increased installation vertical force and torque (Davidson et al., 2022; Tsuha and Aoki, 2010; Ullah et al., 2023). Previous studies have suggested that a multi-helix pile causes more disturbance of the soil during installation because each helix shears the soil in sequence (and more than once) as shown in Fig. 2, and therefore tensile resistance of the upper helices is likely to be reduced for both sand and clay (Lutenegger et al., 2014; Tsuha et al., 2012). However, the effects of introducing extra helices on installation requirements and soil disturbance have not been investigated when considering variation of installation AR.

Additionally, under tensile loading two different theoretical failure mechanisms can occur between helices depending on helix spacing

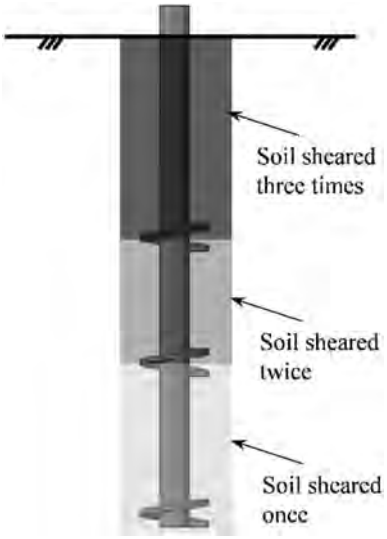

Fig. 2. Schematic diagram of soil disturbance post-installation of a multi-helix pile (after Tsuha et al. (2012)).

(S_h/D_h). When S_h/D_h is large, individual bearing mechanisms occur where the helices mobilise soil individually as separate plate anchors (Fig. 3a). While for smaller S_h/D_h, the development of failure mechanism of the lower helix is restricted by the upper helix and in this case the helices mobilise the soil trapped between them forming a cylindrical soil-soil shear surface (Fig. 3b). Due to the restricted failure mechanism, the cylindrical shearing resistance (Q_{cs}) is expected to be lower than the individual bearing resistance (Q_{ib}). The over-flighting effects on the two mechanisms are potentially different and need to be investigated.

To investigate the efficacy of including more than one helix as well as helix spacing combined with the effect of installation AR in sand, discrete element modelling (DEM) was used to simulate installation and tensile loading tests of a single-helix pile and two piles which have two helices at different spacings. The piles were installed at varying AR values. Overall response and the response of pile components (e.g. base, shaft and each helix) during installation and tensile loading are discussed with the aid of localised stress/strain development and particle movement extracted from the simulations.

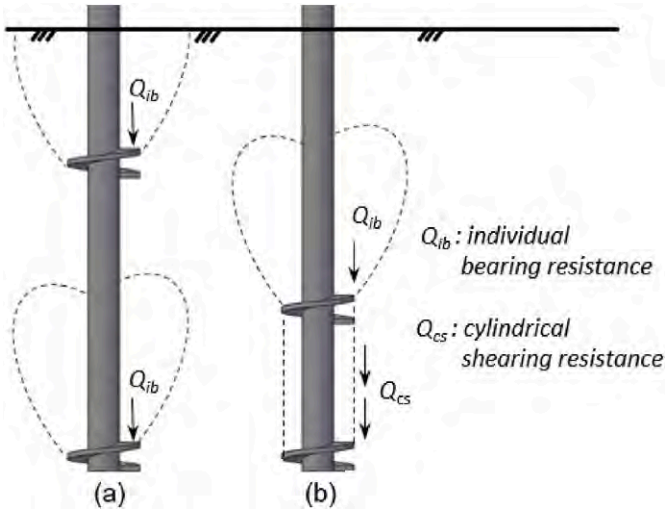

Fig. 3. Schematic diagram of theoretic failure mechanism of screw piles in tension (a) individual bearing (b) cylindrical shearing and bearing above upper helix.

2. Numerical investigation

Commercial software package PFC3D 7.00.159 (Itasca, 2023) was used to simulate screw pile installation and testing in dry soil beds under 50g conditions. This was to allow direct comparison and validation with related model centrifuge testing as described in more detail by Sharif et al. (2021a). Testing in dry sand aimed to simulate drained saturated conditions resulting in the same effective stress regime at 80g in saturated sand such that the scaling factor in this study was set at 80, as per previous centrifuge tests (Davidson et al., 2022; Li et al., 2010) The computing platform adopted was based upon a desktop PC with an Intel® Core CPU i9-10940X @4.1 GHz 14 cores, 32 GB RAM.

2.1. Pile geometry

The geometric parameters of the piles investigated in this study are listed in Table 1. In the pile identification nomenclature, 'nH' indicates helix number being n (S = single, 2 = two) and 'sD' indicates helix spacing, S_h/D_h = s. The single helix pile (SH) has been widely used at the University of Dundee as a benchmark case for experimental (Cerfontaine et al., 2023a; Davidson et al., 2022; Wang et al., 2023b) and in validated numerical studies (Cerfontaine et al., 2021; Sharif et al. 2021a, 2021c; Wang et al., 2023a). This pile was originally designed, by Davidson et al. (2022) (referred to as U1VDB pile), as a single prototype pile at the corner of a four-leg jacket structure in 80 m water depth to support an 8 MW turbine. The double-helix piles in the current study have similar geometry to the single helix pile except with an additional helix (Helix 2, H2) of the same diameter at varying vertical spacing above the first helix (Helix 1, H1) at the bottom. The 2H2D pile was also originally designed and experimentally tested by Davidson et al. (2022) (referred to as U2VD pile). The 2H4D pile had a larger helix spacing. Previous studies suggested a typical critical S_h/D_h = 2–3, representing the transition point between individual bearing and cylindrical shearing (Al-Baghdadi, 2018; Ghazavi et al., 2022; Lutenegger, 2011; Wang et al., 2013). Therefore, between H1 and H2, a cylindrical shearing and individual mechanism were expected for 2H2D and 2H4D, respectively. A helix can be defined as 'shallow' or 'deep' based on if the failure mechanism can develop to the ground surface or not (Ghaly et al., 1991). Based on Cerfontaine et al. (2019), H/D_h = 7.5 for H1 in the current study is just deeper than the transition value from a shallow to deep mechanism in tensile loading. While H/D_h = 5.5 and 3.5 for H2 correspond to shallow mechanism. Note that the installation and helix embedment depth discussed above and listed in Table 1 is only for 'standard' cases. It may differ in some cases and is highlighted in the paper where this is relevant. See Section 2.4 for more detail.

Considering solid steel piles adopted in previous experiments (Davidson et al., 2022; Wang et al., 2023b), the piles in DEM were modelled using rigid wall elements in PFC3D (Itasca, 2023). The pile shaft was divided into eight segments (separate walls) of equal length of 20 mm (1.6 m at prototype scale). Fig. 4 illustrates the reference scheme

Table 1
Geometric parameters for the three piles at prototype scale (installation depth may differ in some cases).

Parameters	Value		
	SH	*2H2D*	*2H4D*
Shaft diameter, D_s (m)	0.88	0.88	0.88
Helix diameter, D_h (m)	1.7	1.7	1.7
Helix pitch, p_h (m)	0.56	0.56	0.56
Helical plate thickness, p_t (m)	0.11	0.11	0.11
Installation depth, L (m)	12.8	12.8	12.8
Embedment depth of the first helix, H_1 (m)	12.24 ($7.5D_h$)	12.24 ($7.5D_h$)	12.24 ($7.5D_h$)
Embedment depth of the second helix, H_2 (m)	–	9.12 ($5.5D_h$)	5.72 ($3.5D_h$)
Helix spacing ratio, S_h/D_h (−)	–	2	4

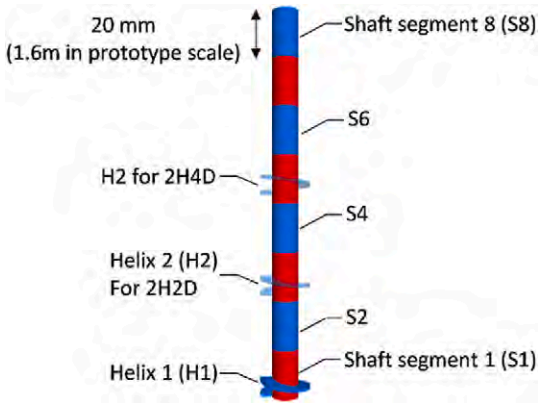

Fig. 4. Arrangement of pile shaft segments relative to the position of helices (each pile only has a maximum of two helices but figure shows both possible positions for Helix H2).

for each shaft segment and their arrangement relative to the positions of helices. Each helix was modelled using a single wall and another circular plate wall was incorporated at the base of the shaft to simulate the closed end (pile base). All the walls used to model the pile shaft and helices were subjected to the same vertical and rotational velocities throughout the simulation to model the pile as a single entity. The "splitting up" of the pile was undertaken to enable the directional contact forces on each of the parts to be assessed independently, similar to an instrumented physical pile.

2.2. Soil bed and contact parameters

The model soil bed generated in this study was based upon the HST95 sand which is widely used at the University of Dundee centrifuge testing and has been extensively characterised through element tests (Al-Defae et al., 2013; Lauder, 2010). Table 2 shows the physical properties of this sand derived from physical characterisation testing. This kind of sand can be described as a uniformly graded with rounded particles.

With respect to DEM simulation based upon the HST95 sand, Sharif et al. (2019) firstly calibrated the particle-particle contact parameters for this type of sand in DEM triaxial simulations that were compared to the results of lab triaxial element tests. Particle shape in DEM models can be considered explicitly by clumping spherical particles (Coetzee, 2017) or implicitly by introducing rolling resistance of spherical particles (Arroyo et al., 2011; Ciantia et al., 2016; Rorato et al., 2021). The latter

Table 2
Physical properties of HST95 sand (Al-Defae et al., 2013; Lauder, 2010).

Properties	Symbol	Value	Value at D_r = 50%
Effective particle size [mm]	d_{10}	0.090	–
Mean particle size [mm]	d_{50}	0.141	–
Largest particle size [mm]	d_{100}	0.213	–
Uniformity coefficient [-]	C_u	1.5	–
Particle roundness [-]	R	0.53	–
Particle density [g/cm^3]	ρ	2.63	–
Minimum void ratio [-]	e_{min}	0.467	–
Maximum void ratio [-]	e_{max}	0.769	–
Dry unit weight [kg/m^3]	γ_{dry}	$14.5 + 3 \times D_r$	16.0
Saturated unit weight [kg/m^3]	γ_{sat}	$18.8 + 1.8 \times D_r$	19.7
Peak friction angle [°]	φ_p	$29 + 20 \times D_r$	39
Peak dilation angle [°]	ψ_p	$-4.4 + 26 \times D_r$	8.6
Critical state friction angle [°]	φ_c	32	–
Steel-sand interface friction angle [°]	δ	24	–

approach allows for the low computational cost usage of a large number of particles that would not be feasible if non-spherical particles were used. In this study, particle shape was introduced by prohibiting rotation of spherical particles as per Arroyo et al. (2011) and Ciantia et al. (2016). Fig. 5 shows a good match between the DEM and experimental triaxial compression response for the soil simulated in this study when adopting this approach. However, for practical application, site specific triaxial test data would be required to calibrate the contact model of the spherical particles if the particle shapes and size distribution varied significantly from those of HST95 sand (see Table 2) that the simulations are based upon. This set of contact parameters was later used for modelling straight-shafted and helical pile testing and particle-pile contact parameters were calibrated by comparison with results of centrifuge tests using HST95 sand (Cerfontaine et al. 2021, 2023b; Sharif et al. 2021a, 2021b, 2021d). Table 3 lists the contact parameters adopted in this study which are consistent with Cerfontaine et al. (2021). The particle-pile (ball-wall) interface friction coefficient μ_p adopted the steel-soil interface friction coefficient was determined using laboratory direct shearing tests by Lauder (2010). This study aims to model a quasi-static condition (da Cruz et al., 2005). In such a case inertial effects are negligible and use of damping is not required (Kozicki et al., 2012). Thus viscous damping was not used in the contact models and critical local damping was set to zero.

Target soil bed porosity in this study was 0.383, which corresponds to HST95 sand in a medium dense state (experimental relative density $D_r = 50\%$). The generation of the soil bed followed the procedure proposed by Sharif et al. (2019) who adopted the particle refinement method (PRM) (McDowell et al., 2012) and periodic cell replication method (PCRM) (Ciantia et al., 2018). PRM was employed to reduce the particle number and consequently overall computational cost. As shown in Fig. 6a, the particle size scaling factor (SF) increased radially in each subzone by 1.4. This chosen value results in d_{50} of an inner zone (i.e. smaller SF) being greater than d_{10} of an adjacent outer zone, to reduce the possibility of particle migration between zones The radius of the central zone was 2.5 D_h allowing for a sufficient zone for the penetrating object and the transference of force from the pile through the various scaled regions. The chosen value was greater than 1.3D_h, within which soil is significantly sheared during installation of a screw pile as shown by Schiavon (2016). The SF in the central zone was 15 leading to $D_s/\ d_{50}$ (where d_{50} is the mean particle diameter) being equal to 5.8 and the effective helix width $w_h = (D_h - D_s)/d_{50} = 2.7$. The adopted SF is adequate to avoid unacceptable particle size effects on installation response and ensures manageable particle numbers (Cerfontaine et al., 2021). Further reduction in SF, say to 10, can lead to prohibitive numbers of particles. The use of PCRM allows faster soil bed generation and improved soil bed homogeneity. This method created the soil bed by assembling representative elementary volumes (REV), which each had radius equal to the size of the final soil bed and a height equal to 3.5 times the diameter of the largest particle in the model as per Sharif et al. (2019). A reduced height would result in arching effects in the radial direction between zones and stress in inner zones being smaller than that in outer zones, as shown by McDowell et al. (2012). The initial single REV was generated at a stress condition matching that at the bottom of the final complete soil bed (e.g. vertical stress $\sigma_v = 310$ kPa and radial stress $\sigma_r = 122$ kPa in this study) (Fig. 6b). The initial REV was radially confined by frictionless wall elements, while in the vertical it was restricted by periodic domain boundaries (particles falling outside of the upper boundary are translated back to the lower boundary and vice versa) (Itasca, 2023), which allowed the initial REV to be replicated vertically to the final whole model height (Fig. 6c) without introducing any unbalanced force into the system. After the replication, the vertical periodic domain was cancelled and movements of particles located at the bottom of the model were prohibited to simulate the bottom of a model box. Finally, the contact force and virtual distance (the virtual contact distance is only for contact force calculation, rather than the physical distance between two objects in contact, see the section titled as *linear model* in PFC3D user's manual for further information (Itasca, 2023)) was scaled based upon the contact laws and desired stress field at 50g conditions (to match the conditions in centrifuge testing) (Fig. 6d) before activating 50g gravity in the model and solving.

In the final soil bed model, frictionless rigid boundaries were created at the bottom of the soil bed and surrounding the circumference. The pile centre was 12D_h from the radial boundary of the soil bed and the pile base (tip) at the end of installation was 11D_h from the bottom boundary to avoid boundary effects as per previous studies (Arroyo et al., 2011; Peng and Yin, 2023).

Table 3
Hertz contact model parameters used in the DEM simulation of HST95 sand (Cerfontaine et al., 2021).

Properties	Symbol	Value
Shear modulus [GPa]	G	3.0
Ball friction coefficient [-]	μ	0.264
Poisson's ratio [-]	ν	0.3
Interface friction coefficient of pile [-]	μ_p	0.445
Local damping [-]	–	0.0
Particle rotation [-]	–	Fixed

2.3. Post-processing of localised soil bed stress states

To process localised stress states, the whole soil bed was partitioned into several annular coaxial cylinders delimited by radial and vertical positions as undertaken by Ciantia et al. (2019) (Fig. 7b). Similar annular and cubic region division approaches for post-processing were also adopted by other previous studies (Rycroft et al., 2009; Theuerkauf

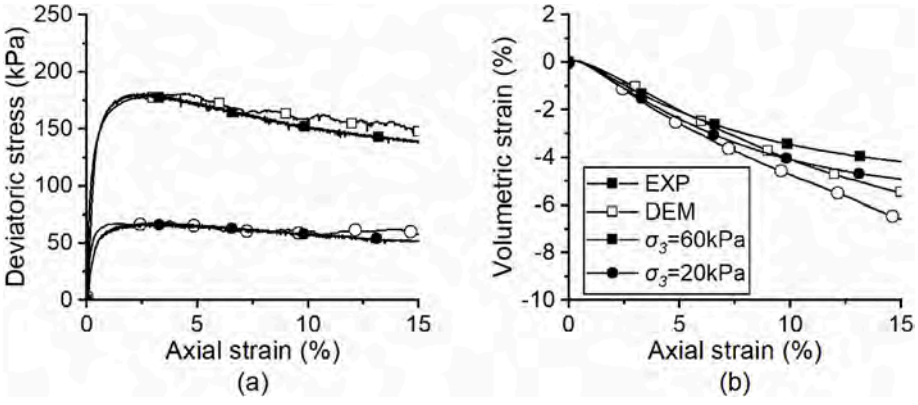

Fig. 5. Comparison of triaxial compression response between DEM and experiments of HST95 sand at $D_r = 50\%$ (a) stress – strain response (b) volumetric strain response.

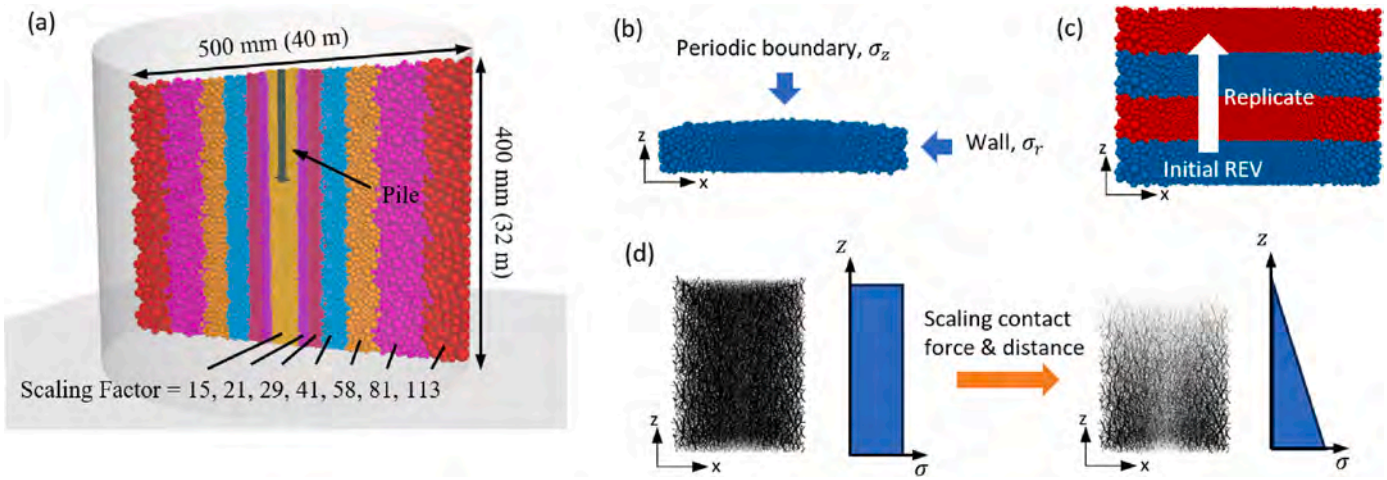

Fig. 6. (a) Half of a soil bed with a screw pile installed (prototype scale in brackets), and (b) schematic representing procedure of periodic cell replication method: generation of the initial REV, (c) cell replication, (d) scaling contact force and contact distance.

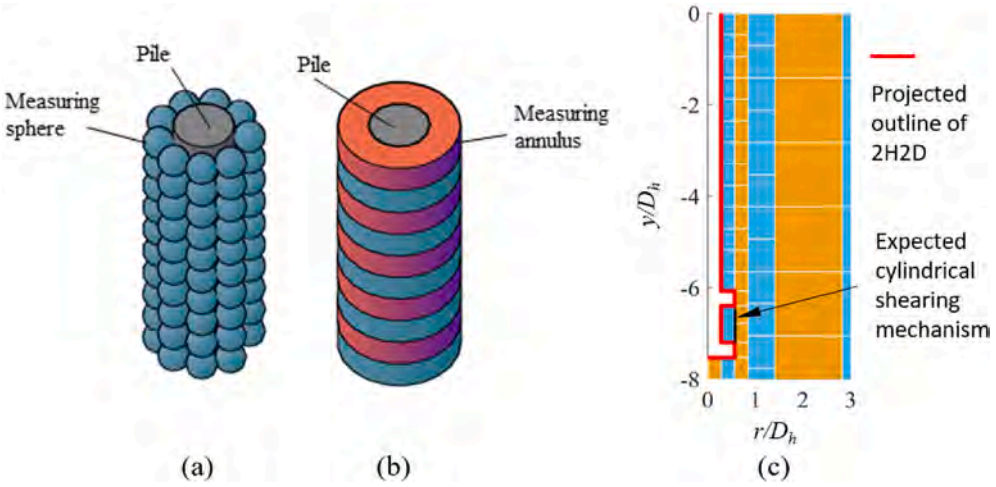

Fig. 7. Schematic comparison between (a) spherical and (b) annular measurement regions applied around a pile and (c) adopted axisymmetric cross section (r is the radial distance from the pile centre, y is the vertical distance from the ground surface).

et al., 2006). Compared to the spherical division approach built into PFC (Itasca, 2023) (Fig. 7a), the approach adopted herein has no overlap between the annular divisions which are assembled to fill the whole model domain, allowing each wall-ball contact on the curved pile-soil interface to be included in one of the measuring regions (Fig. 7b). This method is more suitable for dealing with curved rigid boundaries such as the pile-soil interface in this study. The stress within a region is calculated as the sum of contact force within the region divided by the region volume as is adopted in the PFC measuring sphere approach (Itasca, 2023) and polar coordinates were used instead of Cartesian coordinates. Fig. 7c shows an axisymmetric cross section of the model near to the 2H2D pile as an example, in which each box represents a single annular measuring region adopted in this study. It should be noted that the screw pile is not perfectly axisymmetric due to the helix pitch, therefore in Fig. 7c the pile 'helix' is a projection on the *r-y* plane. The choice of measuring annulus size was set to have a minimum number of 100 particles in any annuli to achieve a statistically representative volume, as well as fit the pile geometry. The width of measuring region in the first column was equal to $0.5D_h$, and it was equal to the helix width, w for the second and third columns. This choice of measuring zone width allows calculation of the stress on the cylindrical shearing surface between the two helices, which will be discussed in Section 4.2, by simply averaging the stress in the three measuring regions on both sides of the cylindrical shear mechanism (Fig. 7c). Fig. 8 shows that stress of the generated soil bed reasonably matches the theoretical in-situ states.

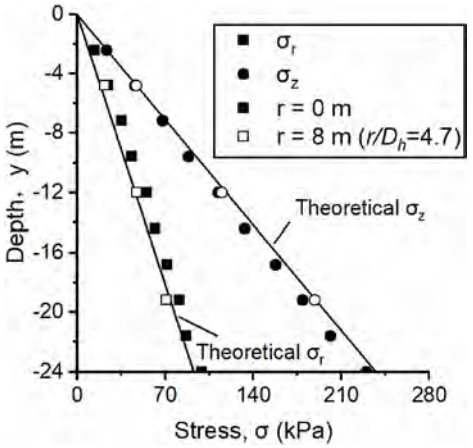

Fig. 8. Stress states of generated soil bed varying with depth at two radial distances compared to the theoretical increase with depth.

2.4. Pile installation and tensile loading tests

To evaluate the effects of AR, pile installation in this study adopted a displacement-controlled approach, where the ratio of pile rotation rate to vertical penetration rate was maintained as constant during a single installation (i.e. constant AR, see Eq. (2)).

Screw pile installation in the field is typically carried out at a rotation rate ranging from 5 to 20 revolutions per minute (Spagnoli and Tsuha, 2020). In previous the centrifuge test, the rotation rate ranged from 2 to 7 revolutions per minute (Schiavon, 2016; Ullah et al., 2023; Wang et al., 2023b). However, within a DEM environment where typical timesteps range between 1×10^{-8} to 1×10^{-6}s (2×10^{-7}s in this study) adopting such a small rotation rate would lead to prohibitively long simulation times. To overcome this intrinsic limitation, the applied rotation rate was maximised while ensuring a quasi-static condition to avoid undesired dynamic effects. Thus, the inertial number I (da Cruz et al., 2005), which represents the ratio of inertial forces of grains to imposed forces and quantifies the significance of dynamic effects on the flow of a granular material, was restricted to 0.01 as recommended by Cerfontaine et al. (2021) who showed further reduction of I had minimal effect on installation response:

$$I = \dot{\gamma} d_{50} \Big/ \sqrt{\rho / p_0'} < 0.01 \tag{3}$$

where $\dot{\gamma}$ is shear strain ratio, d_{50} the mean particle diameter, ρ the particle density, and p_0' the mean effective stress. The quasi-static threshold $I = 0.01$ was also adopted by studies of straight-shafted piles or CPT (Janda and Ooi, 2016; Khosravi et al., 2020).

As detailed in Cerfontaine et al. (2021) the soil shear strain rates $\dot{\gamma}$ for pile installation related to the pile shaft vertical penetration were assumed using Eq. (4) and Eq. (5) (Ciantia et al., 2019; Sharif et al., 2021a):

$$\omega = 2\pi \dot{\gamma} L_{p\omega} / D_h \tag{4}$$

$$v = \dot{\gamma} L_{pv} \tag{5}$$

where ω is rotational velocity and v vertical velocity of installation, $L_{p\omega}$ and L_{pv} are representative dimensions of the plastic deformation zones induced by rotation and vertical movement during the installation and estimated to be $4D_h$ (Galindo et al., 2018) and $3D_h$ (Lu et al., 2004), respectively. Expressing $\dot{\gamma}$ in terms of these quantities, the maximum rotation rate ω_{max} to maintain a screw pile insertion in a quasi-static condition was:

$$\omega_{max} = \min\left(8\pi, \frac{6\pi D_s}{A R p_h}\right) \frac{I}{d_{50}} \sqrt{\frac{p_0'}{\rho}} \tag{6}$$

where inertial number I was assumed to be 0.01 as per above. As ω_{max} is a function of mean effective stress and a centrifuge environment at 50g was modelled, the rotation rate adopted for pile installation increased with depth in order to decrease simulation time.

Fig. 9 shows the ω_{max} corresponding to $I = 0.01$ calculated from Eq. (6). It is compared to the adopted rotational rate, which is increased in a step-wise manner with increase of installation depth. This resulted in a maximum rotation rate during installation of 449 rad/s. The zero stress at soil bed surface results in $\omega_{max} = 0$ at the beginning of installation (when installation depth = 0). To instigate the simulation, $I > 0.01$ was allowed for the first 1 mm (model scale) installation i.e. rotation rate ω for $d_z = 0$–1 mm was equal to ω_{max} at installation depth $d_z = 1$ mm as shown in Fig. 9. Once the rotational rate is determined, the vertical penetration rate can be obtained from Eq. (2) based upon the pile geometry and the target AR values. The maximum vertical penetration rate ranged from 0.125 to 0.5 m/s with AR increasing from 0.25 to 1.0. Butlanska et al. (2010) simulated cone penetration tests in a calibration chamber condition (average stress = 72 kPa) and showed the results

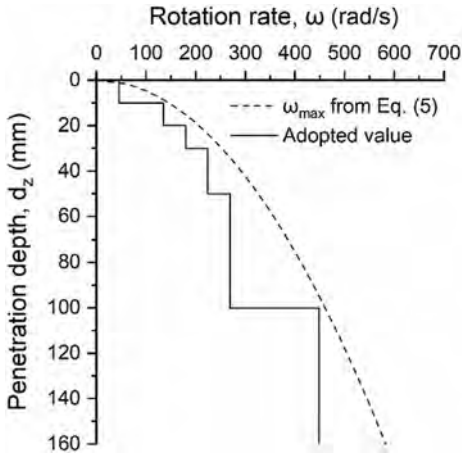

Fig. 9. Rotation rate adopted during installation compared to the allowance calculated by Eq. (6) (at model scale).

were insensitive to penetration rate within a comparable range of 0.02–0.5 m/s.

After the piles penetrated to the target depth, tensile loading tests were undertaken in which the piles were uplifted monotonically at a constant velocity of 0.1 m/s (model scale) to a vertical displacement of $0.1D_h$.

2.5. Summary of simulations conducted

In this study, the three piles were installed at AR = 1.0, 0.5 and 0.25. Table 4 summaries simulations conducted. The pitch-matched installation (AR = 1.0) is recommended by current standards but may not be practical for offshore application due to requirement of large compressive installation forces (Davidson et al., 2022). Installation at AR = 0.25 was suggested to create a tensile installation force, which allows the pile to effectively pull itself into ground and create optimal tensile capacity for the single-helix pile SH (Cerfontaine et al., 2023a). Installation at AR = 0.5 (Test 7) was only used for the 2H2D pile to allow discussion of the cylindrical shearing between two helices and the results are only presented in Section 4.2. In Simulation 1 to 8, piles were installed to a standard depth where the first (bottom) helix embedment depth ratio $H_1/D_h = 7.5$. The SH pile was installed to shallower depth at both AR = 1.0 and 0.25 (Test 8–11), to evaluate soil disturbance induced by multiple helix passage (Section 4.3). The SH and 2H2D piles were installed to a greater depth at AR = 0.25 in Test 12 and 13 to discuss the effect of deep/shallow failure transition with respect to helix number on tensile capacity (Section 5).

3. Helix spacing effect on installation

3.1. Overall installation requirements

Fig. 10 shows the overall installation requirements for single-helix pile SH and double-helix piles 2H2D and 2H4D in DEM, alongside the installation requirements measured for SH by Wang et al. (2023b) in centrifuge tests referred to as EXP. For installation vertical force in this study, a positive value is assigned to compressive forces. Although torque for SH installed at AR = 0.25 is slightly underestimated, DEM reasonably reproduces AR effects on installation requirements. That is, reducing AR results in reduced vertical compressive force (and can even create tensile force on the loading rig) and torque (Cerfontaine et al. 2021, 2022, 2023a; Sharif et al. 2021a, 2021c; Wang et al., 2023b).

Fig. 10 also suggests that both installation vertical force and torque vary with helix number and spacing. For piles installed following the pitch-matched approach (AR = 1.0), introduction of the second helix (H2) leads to an increase in both vertical force and torque during

Table 4
Summary of simulations conducted.

Simulation number	Pile ID	AR	First (bottom) helix embedment depth ratio, H_1/D_h	Final installation force, F (MN)	Final installation torque, T (MNm)	Tensile capacity, Q_t (MN)
1	SH	1.0	7.5	10.8	2.62	7.25
2	SH	0.25	7.5	−1.75	3.48	10.63
3	2H2D	1.0	7.5	12.04	3.76	8.23
4	2H2D	0.25	7.5	−1.48	3.23	8.46
5	2H4D	1.0	7.5	11.31	3.04	8.62
6	2H4D	0.25	7.5	−2.17	3.49	10.04
7	2H2D	0.5	7.5	2.23	3.55	9.5
8	SH	1.0	3.5	5.27	1.04	2.71
9	SH	0.25	3.5	0.08	0.55	3.95
10	SH	1.0	5.5	8.55	1.70	6.41
11	SH	0.25	5.5	−1.0	1.72	7.30
12	SH	0.25	10.4	−3.82	6.57	12.5
13	2H2D	0.25	10.4	−3.22	6.02	13.8

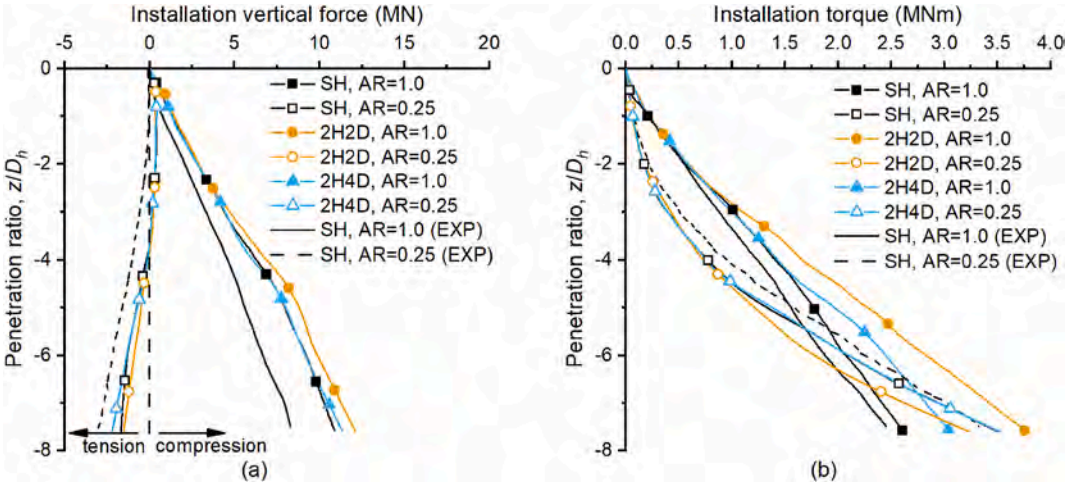

Fig. 10. Overall installation requirements for single and dual-helix piles (a) vertical force, (b) torque.

installation. The extent of these increments diminishes as the helix spacing widens due to decrease of embedment depth of H2. Davidson et al. (2022) investigated SH and 2H2D at AR = 1.0 but in denser HST95 sand (D_r = 82%) and suggested that installation compressive force of 2H2D is marginally higher (8%) than SH at the end of installation, comparable to the 11% increase predicted in the current DEM study

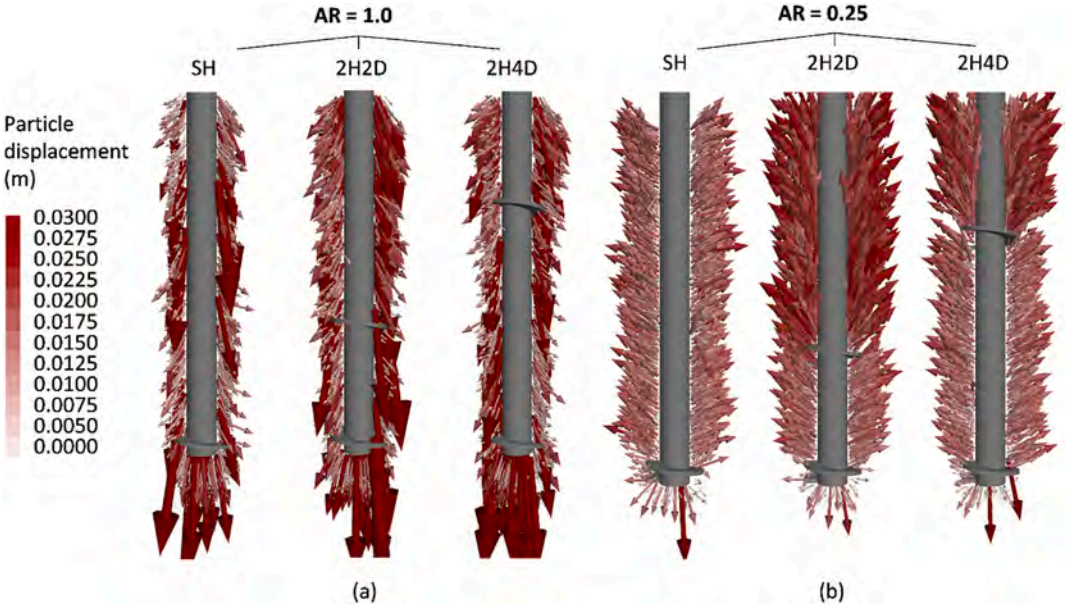

Fig. 11. Helix spacing effects on displacement of particles around screw piles at the end of installation for (a) pitch-matched installation at AR = 1.0 (b) over-flighted installation at AR = 0.25.

(Fig. 10a). In terms of torque, Fig. 10b shows that required installation torque of 2H2D and 2H4D is 20% and 15% higher than SH, respectively. The torque increase by 20% from SH to 2H2D also reasonably matches Davidson et al. (2022) who suggested 20% although the soil relative density was higher than in this study.

For the piles installed using the over-flighted approach (AR = 0.25), Fig. 10 indicates that the torque and tensile force required during installation of 2H2D is lower than the rest of two cases. For instance, torque for 2H2D at the end of installation is 1.44 MNm and 26% lower than SH. The potential of reduced installation requirements induced by inclusion of additional helices during over-flighting contrasts with pitch-matched installation where installation requirements typically increase with helix number as per the current and previous studies (Davidson et al., 2022; Tsuha and Aoki, 2010; Ullah et al., 2023).

3.2. Post-installation particle movement and stress field

To understand the controlling mechanisms during installation, the particle displacement and post-installation stress field are analysed. Fig. 11 depicts the displacement vectors of particles within a radial distance of 1 D_h from the pile centre, extending from 1 D_h below the pile base to 1 D_h above H2 of 2H4D. For the piles installed at AR = 1.0 (Fig. 11a), particles are displaced downwards and outwards and no significant difference is seen with varying helix spacing. In terms of over-flighted piles (Fig. 11b), installation at AR = 0.25 displaces particles upwards as observed by Cerfontaine et al. (2021) and Sharif et al. (2021a), and, compared to AR = 1.0, there is less scatter among displacement vectors and more of an outwards displacement trend. It is also noticeable that helix spacing has an effect on particle displacements when over-flighting. For the dual helix piles, the particle displacement between the first helix (H1) and the second helix (H2) is comparable to the single-helix case but the particles above H2 exhibit greater upwards and outwards displacement.

The variation of particle displacement modes due to AR and helix spacing results in variation of stress field. Figs. 12 and 13 depict vertical stress (σ_z) and radial stress (σ_r) fields, respectively, around the three piles after installation at both AR = 1.0 and 0.25. The influence of AR and helix number/spacing on the stress fields is similar for both σ_z and σ_r. Therefore, in this section, 'stress' refers to both σ_z and σ_r if not specified separately. The impact of variation of AR on the single-helix pile (SH) is consistent with Sharif et al. (2021a). During installation at AR = 1.0, soil particles are pushed downwards (Fig. 11a), increasing the stress beneath and adjacent to the helix and creating a low stress zone above it. It is possible to mitigate this phenomenon by over-flighting (AR < 1.0) since soil particles are translated upward as shown in Fig. 11b. This is also true for dual-helix piles but the helix spacing makes

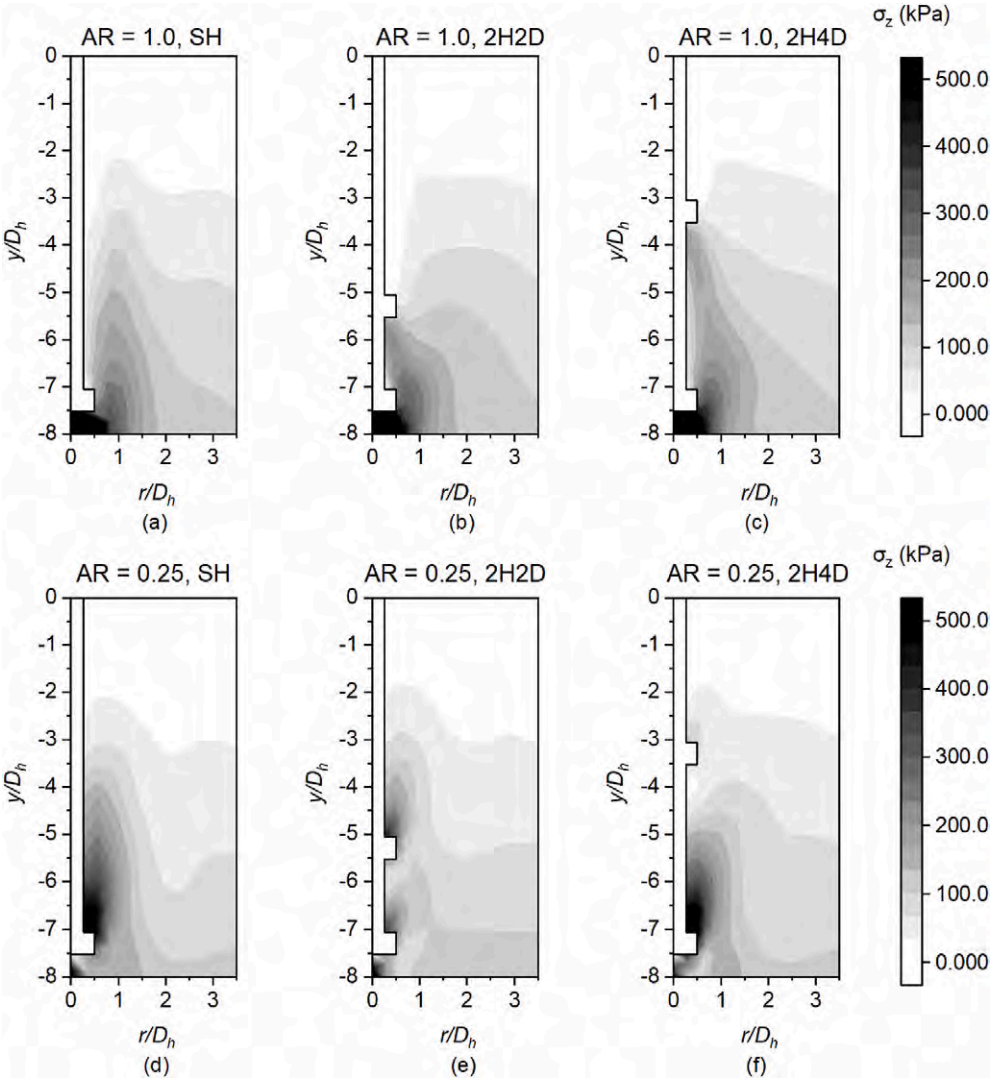

Fig. 12. Post-installation vertical stress (σ_z) field around piles with varying helix spacing installed at varying AR (AR = 1.0 and 0.25): (a) SH, (b) 2H2D, (c) 2H4D for AR = 1.0 and (d) SH, (e) 2H2D, (f) 2H4D for AR = 0.25 (r is the radial distance from the pile centre, y is the vertical distance from the ground surface).

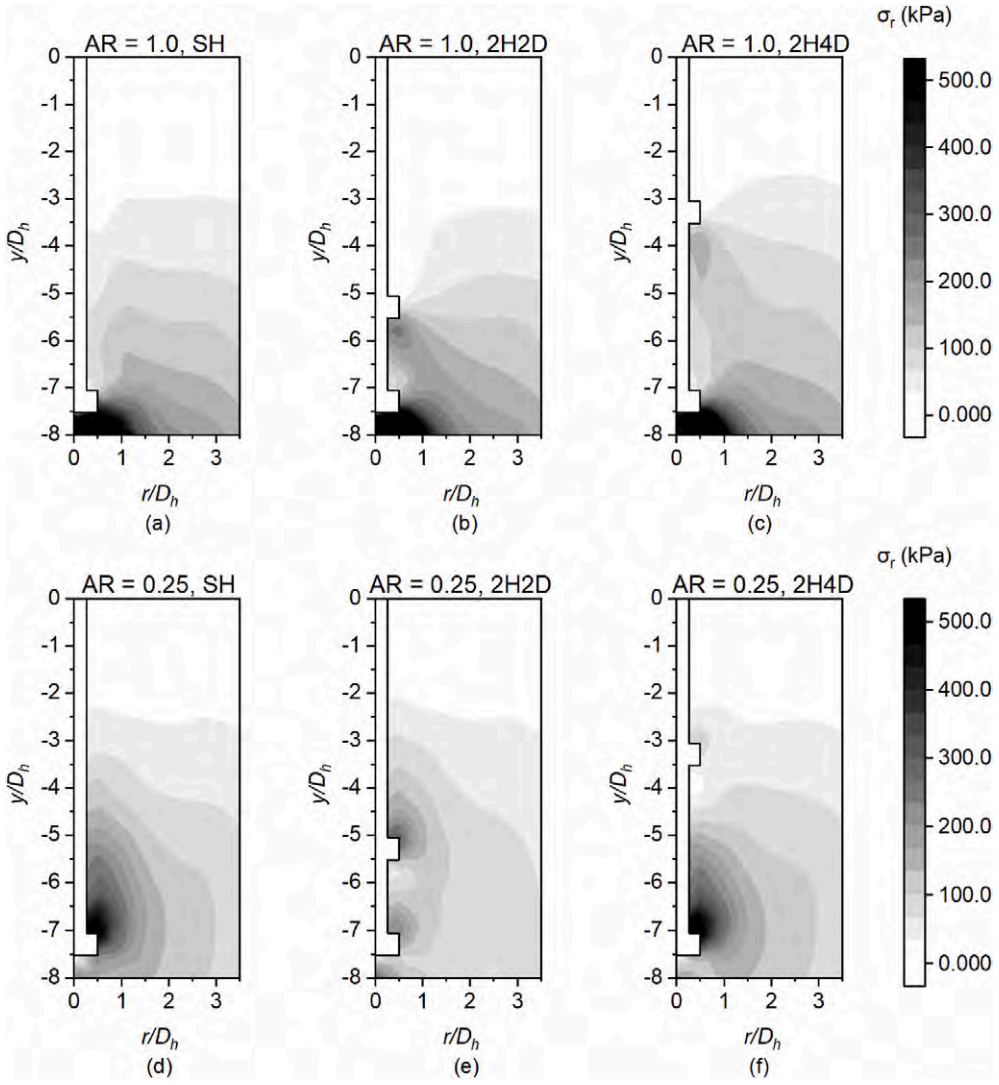

Fig. 13. Post-installation radial stress (σ_r) field around piles with varying helix spacing installed at varying AR (AR = 1.0 and 0.25): (a) SH, (b) 2H2D, (c) 2H4D for AR = 1.0 and (d) SH, (e) 2H2D, (f) 2H4D for AR = 0.25 (r is the radial distance from the pile centre, y is the vertical distance from the ground surface).

a difference. Based upon the stress fields, the 2H4D pile behaves very similarly to the single helix pile (for both AR = 1.0 and 0.25), and the zone influenced by second helix (H2) does not propagate all the way to the first helix (H1). However, in case of 2H2D, H1 "constrains" the global stress fields and draws the stress down to H2. Specifically, for the case of 2H2D, AR = 0.25, the stress above H1 is significantly reduced by

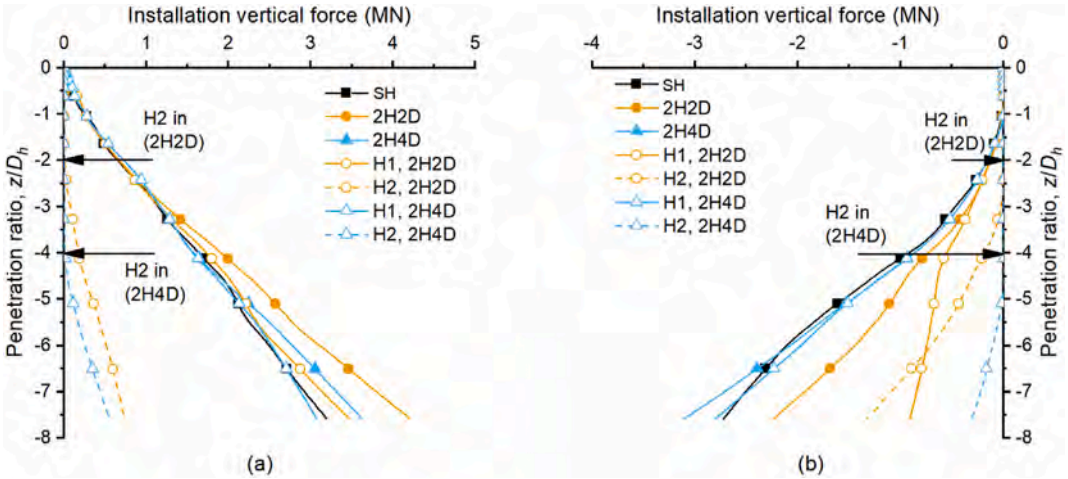

Fig. 14. Installation vertical force measured at the helices (a) AR = 1.0 (b) AR = 0.25.

H2 when compared to the single helix case.

3.3. Installation requirements measured on pile components

With the aid of the post-installation stress field, it is possible to explain the variation of installation vertical force and torque measured on each pile component and provide insights into how to aid optimised installation. Both installation vertical force and torque on the pile base is significantly reduced by reducing AR in line with Sharif et al. (2021c), but it is not affected by helix number and spacing therefore is not presented here.

3.3.1. Vertical force and torque measured on the helices

Fig. 14a and (b) presents the installation vertical force on the helices for AR = 1.0 and AR = 0.25, respectively. For dual-helix piles, the force on each helix and the total force are shown separately.

For the pitch-matched cases (AR = 1.0, Fig. 14a), the second helix (H2) does not induce variation of vertical force on the first helix (H1). Therefore, the limited difference in total force (Fig. 10a) between the two cases is a result of the late involvement of H2, resulting in higher total helix force at a given penetration depth for the 2H2D case.

In terms of the over-flighted cases (AR = 0.25, Fig. 14b), the presence of the second helix (H2) does not affect vertical force on the first helix (H1) for the larger helix spacing (2H4D). When S_h/D_h reduces to 2 (2H2D), however, vertical force on H1 is lower than SH and 2H4D and the final vertical force on H2 exceeds that on H1. Although the deeper H2 of 2H2D results in higher tensile force on itself compared to 2H4D, the total vertical helix force on 2H2D is lower than 2H4D and even SH (Fig. 10a). This is consistent with the low stress zone between the two helices of 2H2D, AR = 0.25 (Figs. 12e and 13e).

The helix spacing effect on installation torque, as shown in Fig. 15, is similar to that on vertical force. At AR = 1.0 there appears to be little effect of the second helix (2H) on the behaviour of the first helix (H1) for either spacing (2H2D and 2H4D). However, for AR = 0.25, torque on H1 is reduced, in line with the low stress zone between the two helices of 2H2D (Figs. 12 and 13). When S_h/D_h = 4 (2H4D) the torque on H1 remains almost unaffected compared to the single helix case (SH).

3.3.2. Torque measured on shaft at varying depths

Figs. 16 and 17 present installation torque on three selected shaft segments (Fig. 4) of the three piles installed at AR = 1.0 and 0.25, respectively. For AR = 1.0, the presence of the second helix (H2) enhances and reduces torque on the shaft segments below and above it, respectively, associated with the variation of soil radial stress (Fig. 13). For 2H2D, the torque on the shaft segment S2, which is between the first helix (H1) and H2, is enhanced compared to the single helix case (SH), while for 2H4D where S2 is $2D_h$ below H2 there is no significant difference (Fig. 16a). When considering segment S4, it is notable that the passage of H2 of 2H2D reduces the torque at S4 over that of the single helix case (SH), while for the 2H4D case the S4 torque is increased over the SH case as H2 pushes soil downwards to this zone (Fig. 11a) and increases the soil radial stress (Fig. 13c). Segment S6 (Fig. 16c), which is above all of the helices, exhibits generally similar torque readings although the additional helix cases have slightly lower torque than the SH.

For the AR = 0.25 case there is a reversal of behaviour that installation torque on the segments below H2 tend to decrease while above tends to increase. The torque reduces in S2 for the 2H2D case and minor changes are seen for the 2H4D case (Fig. 17a). This is a result of reduced stress in this zone as H2 over-flights and removes material from this area to push it up above H2 (Figs. 11b and 13e). This also results in increased torque on segment S4 above H2 of 2H2D (Fig. 17b). For 2H2D this segment is below H2 therefore the torque is reduced as particles are removed resulting in reduced radial stress. In terms of S6 which is above all helices, the torque is slightly increased over the single-helix case (SH).

4. Helix spacing effect on monotonic tensile response

4.1. Failure mechanism and tensile resistance measured on each helix

As well as the need to optimise installation, in-service performance also needs to be considered as this is expected to be influenced by helix spacing/number and as previously shown AR. Fig. 18 compares the failure mechanism of each pile installed at AR = 1.0 and 0.25, by plotting particle vertical displacements at a tensile displacement of 0.1 D_h i.e. 0.17 m (at prototype scale). For comparison, the potential shallow failure wedge propagating upwards inclined at the dilation angle ψ_p assumed by Giampa et al. (2017) is also shown as red dashed lines.

When assessing the single-helix piles (SH) installed at AR = 1.0 (Fig. 18a), the failure appears not to be fully developed to the ground surface suggesting a predominantly deep mechanism. However, when AR is reduced to 0.25 (Fig. 18d), the failure mechanism widens, in agreement with Sharif et al. (2021a), and tends towards the assumed shallow failure mechanism, showing a transitional state between deep and shallow mechanisms. The failure mechanism transfer supports the assumption that the helix embedment depth is close to the transitional depth (Section 2.1).

For the dual-helix piles, for both AR = 1.0 and 0.25, the intensive and relatively uniform displacement between H1 and H2 at a spacing of

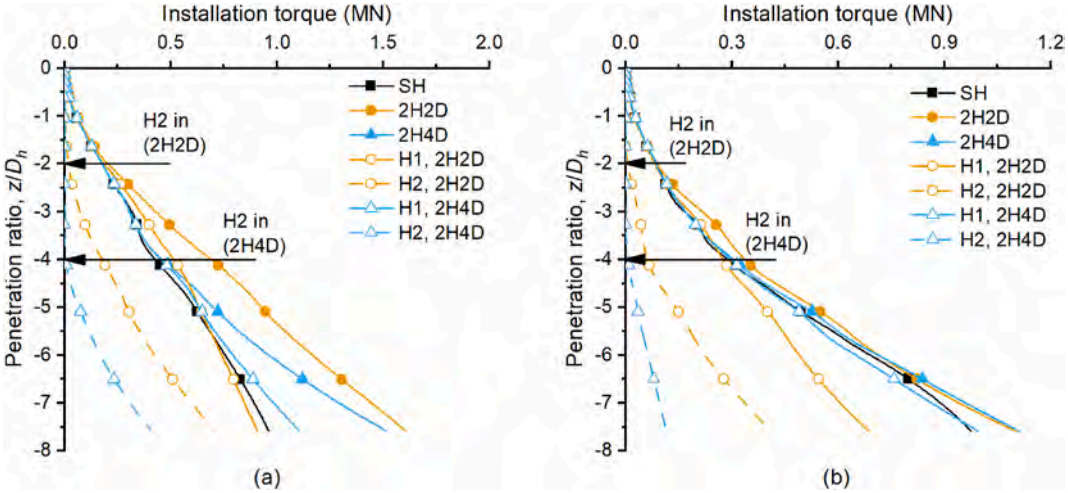

Fig. 15. Installation torque measured at the helices (a) AR = 1.0 (b) AR = 0.25.

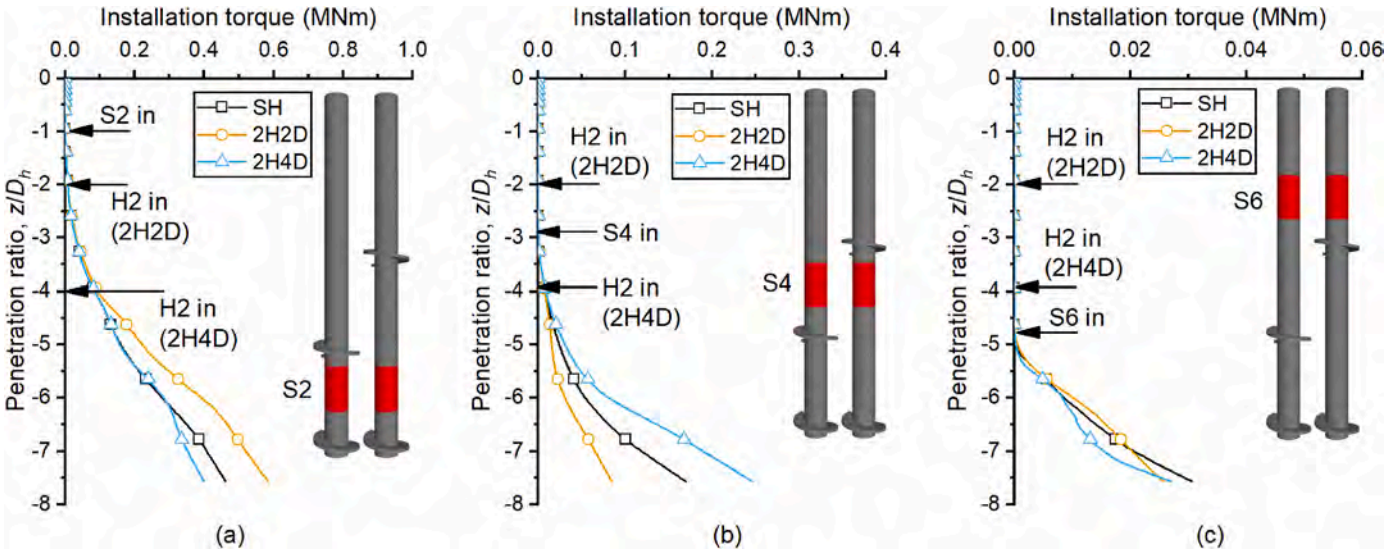

Fig. 16. Installation torque on selected shaft segments for AR = 1.0 (a) Segment 2, (b) Segment 4 and (c) Segment 6.

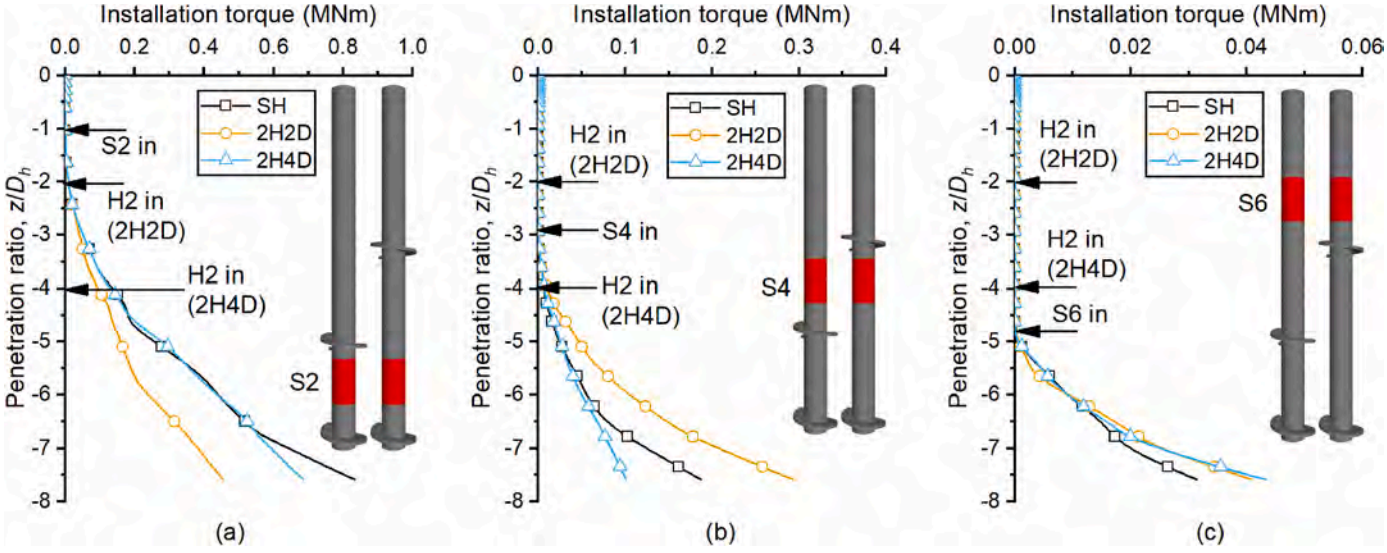

Fig. 17. Installation torque on selected shaft segments for AR = 0.25 (a) Segment 2, (b) Segment 4 and (c) Segment 6.

$S_h/D_h = 2$ suggests a cylindrical shear mechanism (Fig. 18b and e), while when the helix spacing is greater (2H4D) the individual bearing mechanism is seen (Fig. 18c and f). This is in line with the transition of mechanisms noted by several other previous studies which often refer to transition between 2–3 S_h/D_h as discussed previously.

Table 5 summaries tensile capacity Q_t, defined as resistance at the ultimate uplift displacement of $0.1D_h$, of each case with different installation AR values and helix spacings. The tensile capacity measured on helices and pile shaft separately, along with its proportion of the total capacity, is also listed. The scenario of AR = 0.5, 2H2D will be confined to the discussion of cylindrical failure mechanisms between the two helices (Section 4.2) and will not be utilised elsewhere in this paper.

Fig. 19a shows helix spacing effects on tensile capacity Q_t. In terms of AR = 1.0, dual-helix piles have larger Q_t than the single helix pile (SH). While for AR = 0.25 introduction of the second helix is not necessarily beneficial as the tensile capacity is not enhanced and can even be lower, although the installation benefits from reduced AR (see Fig. 10) which might offset this reduction depending on the application. The reverse observation between AR = 1.0 and 0.25 is attributed to the different failure mechanism of SH as shown in Fig. 18. The deep failure mechanism of SH installed at AR = 1.0 (Fig. 18a) allows an additional upper helix to mobilise more soil (Fig. 18b and c) and subsequently enhance the overall tensile capacity (Fig. 19a). While for AR = 0.25, the shallow or transitional failure mechanism of the first helix developing to the ground surface (Fig. 18d) prevents the second helix from increasing the volume of the failure mechanism (Fig. 18e and f), resulting in a similar tensile capacity to the single-helix case (Fig. 19a). Even for the smaller S_h/D_h, the form of cylindrical shearing mechanism between H1 and H2 decreases the overall failure mechanism and reduces the overall tensile capacity. However, it can be inferred that if the over-flighted piles are installed to a greater depth where H1 can exhibit a deep mechanism, an improved tensile capacity of the dual-helix piles over the single-helix pile can be observed. It also suggests that it is necessary to consider the deep/shallow mechanism transition induced by adopting different installation AR values when trying to enhance tensile capacity of screw pile by adopting additional helices. For either AR = 1.0 or 0.25, 2H2D has a lower tensile capacity than 2H4D. It suggests that lower helix-spacing may be avoided for optimised tensile capacity of multi-helix piles.

Fig. 19b evaluates the tensile capacity of the two helices separately.

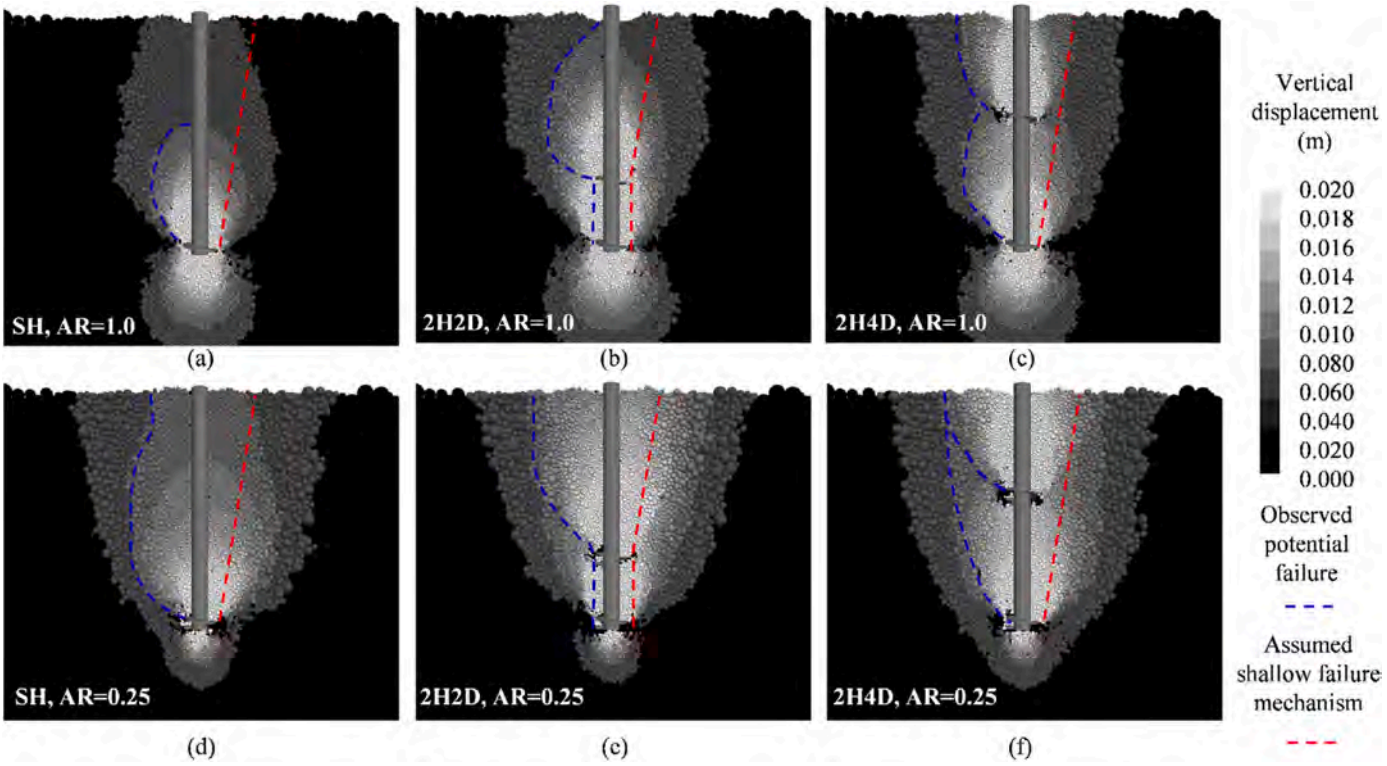

Fig. 18. Comparison of failure mechanism of screw piles with varying helix spacing S_h and installed at AR = 1.0 and 0.25 (a) SH, AR = 1.0; (b) 2H2D, AR = 1.0; (c) 2H4D, AR = 1.0; (d) SH, AR = 0.25; (e) 2H2D, AR = 0.25; (f) 2H4D, AR = 0.25 (H1 installed to $H/D_h = 7.5$ s).

Table 5
Tensile capacity of single-helix and double-helix piles installed at AR = 1.0 and 0.25 (component proportions of total capacity in brackets, all shown at prototype scale).

Installation mode	Pile	Resistance measured on (MN)			Total capacity, Q_t (MN)
		H1	H2	Shaft	
AR = 1.0	SH	6.22 (86%)		1.03 (14%)	7.25
	2H2D	4.68 (57%)	2.60 (32%)	0.95 (11%)	8.23
	2H4D	6.41 (74%)	1.09 (13%)	1.12 (13%)	8.62
AR = 0.25	SH	9.41 (88%)		1.22 (12%)	10.63
	2H2D	2.91 (34%)	4.43 (53%)	1.12 (13%)	8.46
	2H4D	7.72 (77%)	1.38 (14%)	0.94 (9%)	10.04
AR = 0.5	2H2D	3.75 (39%)	4.70 (50%)	1.05 (11%)	9.50

A dimensionless helix resistance factor (or breakout factor) N_γ is used (Meyerhof and Adams, 1968):

$$N_\gamma = \frac{4Q_h}{\pi {D_h}^2 H\gamma'} \tag{7}$$

where Q_h is tensile capacity of a helix, D_h is the helix diameter, H is the helix embedment depth, and γ' is in-situ effective unit weight of soil above the helix (prior to installation). Fig. 19b indicates that, for the first helix (H1), there is a trend for reduction of N_γ with reducing S_h/D_h in line with transfer from individual bearing to cylindrical shearing mechanism observed in Fig. 18. However, when $S_h/D_h = 2$, N_γ of AR = 0.25 is even lower than N_γ of AR = 1.0 which is the opposite of the observation made by previous studies which suggested increased N_γ due to reduction of AR (Cerfontaine et al., 2023a; Sharif et al., 2021a). This is attributed to the installation induced variation of stress field as shown in Figs. 12 and 13 as well as a transition from an individual bearing capacity mechanism to a cylindrical one as is often assumed (Fig. 3) (further discussed in Section 4.2). When assessing the second helix (H2), reducing AR simply leads to higher N_γ in line with observation on single-helix piles made by Cerfontaine et al. (2023a) and Sharif et al. (2021a).

4.2. Over-flighting effects on cylindrical shearing resistance

As shown in Fig. 18(b and e) a cylindrical shearing mechanism occurs for the 2H2D pile for both AR = 1.0 and 0.25. The cylindrical shearing resistance is theoretically equal to the soil-soil friction resistance between the soil trapped between the two helices and surrounding soil such that the cylindrical shear resistance Q_{cs} can be calculated as (Mitsch and Clemence, 1985):

$$Q_{cs} = \sigma_v' K tan\varphi_p' \pi D_h (H_1 - H_2) = \sigma_r' \, tan\, \varphi_p' \pi D_h (H_1 - H_2) \tag{8}$$

where σ_v' and σ_r' are the effective vertical and radial stresses on the cylindrical shear surface, K is the coefficient of passive lateral earth pressure during uplift, φ_p' is the effective peak friction angle of the soil, D_h is the helix diameter, and $H_1 - H_2$ is the vertical distance between the two helices. For a given pile geometry, Q_{cs} is a function of σ_r' and φ_p'. In typical design, σ_v' is considered as the in-situ value and K is derived from empirical relationships which may consider installation effects to some degree (Das and Shukla, 2013). Mitsch and Clemence (1985) suggested K can be calculated from:

$$K = 0.6 + mH_2/D_h \tag{9}$$

where m is an empirical factor presented in Table 6. For $\varphi_p' = 39°$ in this study (Table 2), the corresponding $K = 1.98$.

Fig. 20a shows the Q_{cs} directly measured in DEM (resistance below

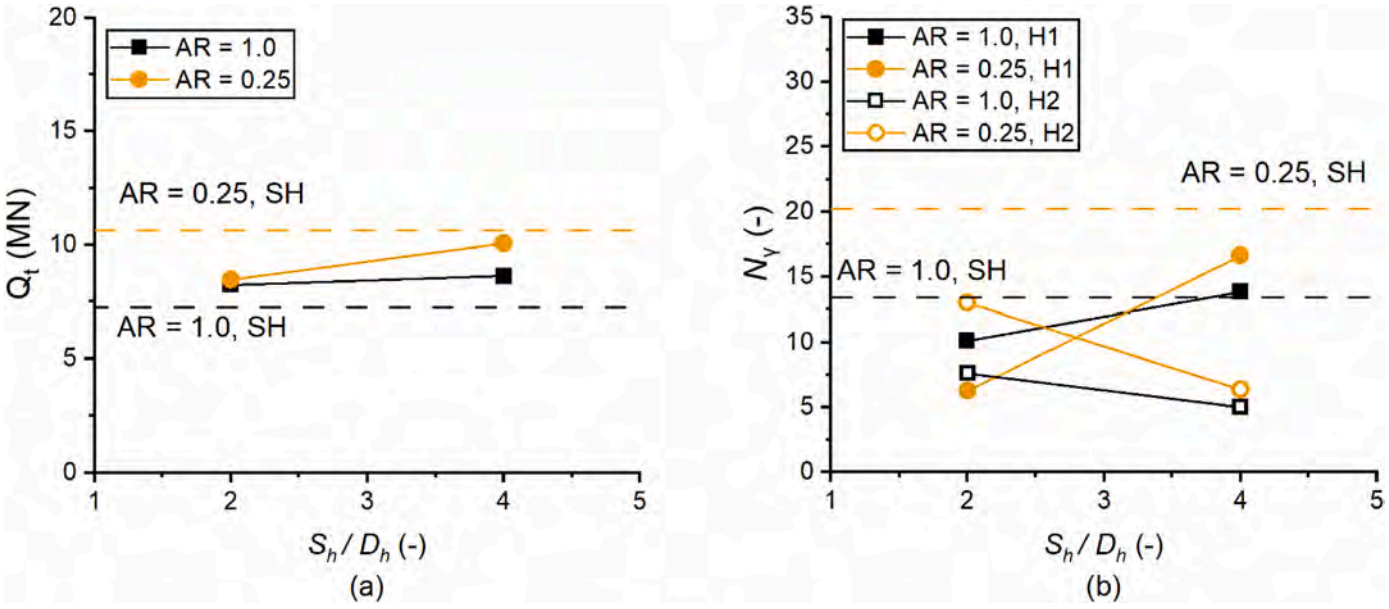

Fig. 19. Effects of AR and S_h/D_h on tensile response (a) total tensile capacity (b) resistance factor N_γ of each helix.

Table 6
Values of m for various soil friction angles φ_p', as derived by Mitsch and Clemence (1985).

φ_p' (°)	m
25	0.033
30	0.075
35	0.180
40	0.250
45	0.289

H2, i.e. sum of tensile resistance measured on H1 and the shaft between H2 and H1), compared to Q_{cs} predicted by Eq. (8) adopting different input parameters. As expected, adopting theoretical in-situ (prior to pile installation) σ_r' on the assumed cylindrical shearing interface leads to significant underestimation of Q_{cs} (dot dashed line in Fig. 20a). Using the K value proposed by Mitsch and Clemence (1985) gives a more reasonable prediction with some attempt to reflect installation effects, although this method does not directly consider the influence of installation AR (dashed line in Fig. 20a). Alternatively, σ_r' directly extracted from DEM can be input into Eq. (8) to evaluate the AR effects (solid circle symbols). As expected, the DEM post-installation σ_r' prior to the tensile loading also underestimates Q_{cs} as the loading induced stress state variation is not considered (i.e. passive lateral earth pressure is typically higher than lateral earth pressure at rest), although it reproduces the trend of decreased Q_{cs} with reduction of AR. Adopting the DEM σ_r' at a tensile displacement at 0.1 D_h (where tensile capacity is measured) gives a better result (open circle symbols). Fig. 20b shows the m value back-calculated based on the measured resistance below H2 (solid square data points in Fig. 20a), which also reduces with decreased AR as expected. It again suggests a necessity for consideration of AR for Q_{cs} calculation.

4.3. Over-flighting effects on soil disturbance induced by extra helix passage

Previous studies have suggested that multi-helix screw piles tend to cause more disturbance of the soil than single-helix piles during installation at AR = 1.0 (Lutenegger et al., 2014; Tsuha et al., 2012) as discussed previously. Based on this assertion the tensile resistance of H2 of the dual-helix piles in this study should be influenced by penetration of

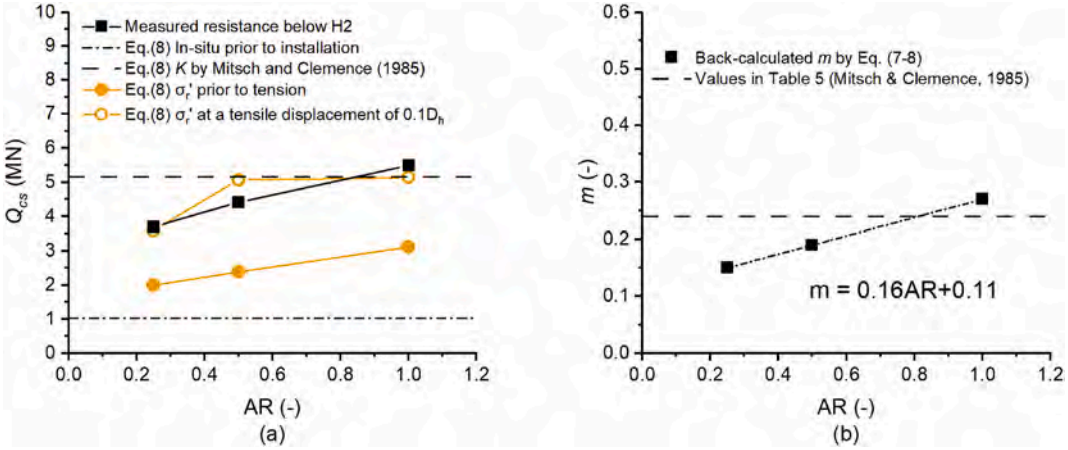

Fig. 20. Comparison of theorietical and measured cylindrical shear resistance between H1 and H2 with variation of AR (a) Q_{cs} calculated adopting input parameters derived from emprical relationships and DEM, (b) back-calculated value of m factor based on DEM measurements.

H1. To evaluate this effect, the single-helix pile (SH) was installed to the depth of H2 of 2H2D (5.5 D_h) and 2H4D (3.5 D_h) followed by tensile loading tests.

Fig. 21 compares post-installation vertical stress of the partially penetrated single-helix cases to the corresponding two-helix cases. It indicates, for both AR = 1.0 and 0.25, that the vertical stress in the case of dual-helicx pile exhibits a reduction compared to single helix. The disturbance of soil above the second helix (H2) induced by penetration of H2 can be also interpreted by variation of tensile resistance of the helix. Fig. 22 compares the helix resistance factor N_γ of H2 of the dual-helix piles (open symbols in Fig. 19b) to the single-helix piles with the same helix embedment depth of H2 (5.5D_h for 2H2D and 3.5D_h for 2H4D as shown in Fig. 21). It shows that multiple helix passage (H2) results in smaller N_γ than one passage. In addition, over-flighted installation leads to smaller N_γ reduction (2%–12%) from single to H2 than installation AR = 1.0 (30%–33%). But in the case of 2H2D, AR = 0.25, the reduced soil disturbance above H2 does not compensate for the detrimental effects of the low stress between the helices (H1 and H2) which results in lower overall tensile capacity (Fig. 19). The lesser reduction of the tensile resistance of the second helix induced by over-flighting needs to be considered for design.

5. Effect of installation depth for over-flighted piles (AR = 0.25)

It has been shown in Section 4.1 ($H_1/D_h = 7.5$) that, at installation AR = 0.25, the dual-helix (2H2D and 2H4D) piles do not develop improved but lower tensile capacity than the single helix pile (SH), because the first helix H1 already develops a shallow failure which cannot be extended by additional helices (Fig. 18). However, as shown in Fig. 23, if the piles are installed deeper to $H_1/D_h = 10.4$ where the SH exhibits a deep failure mechanism, for example the 2H2D pile can mobilise more soil and create an improved tensile capacity. In addition, the decreased installation torque of 2H2D compared to SH remains. Thus, it is also possible to improve tensile capacity and reduced installation torque of over-flighted piles by inclusion of additional helices if the H1 failure mechanism is deep.

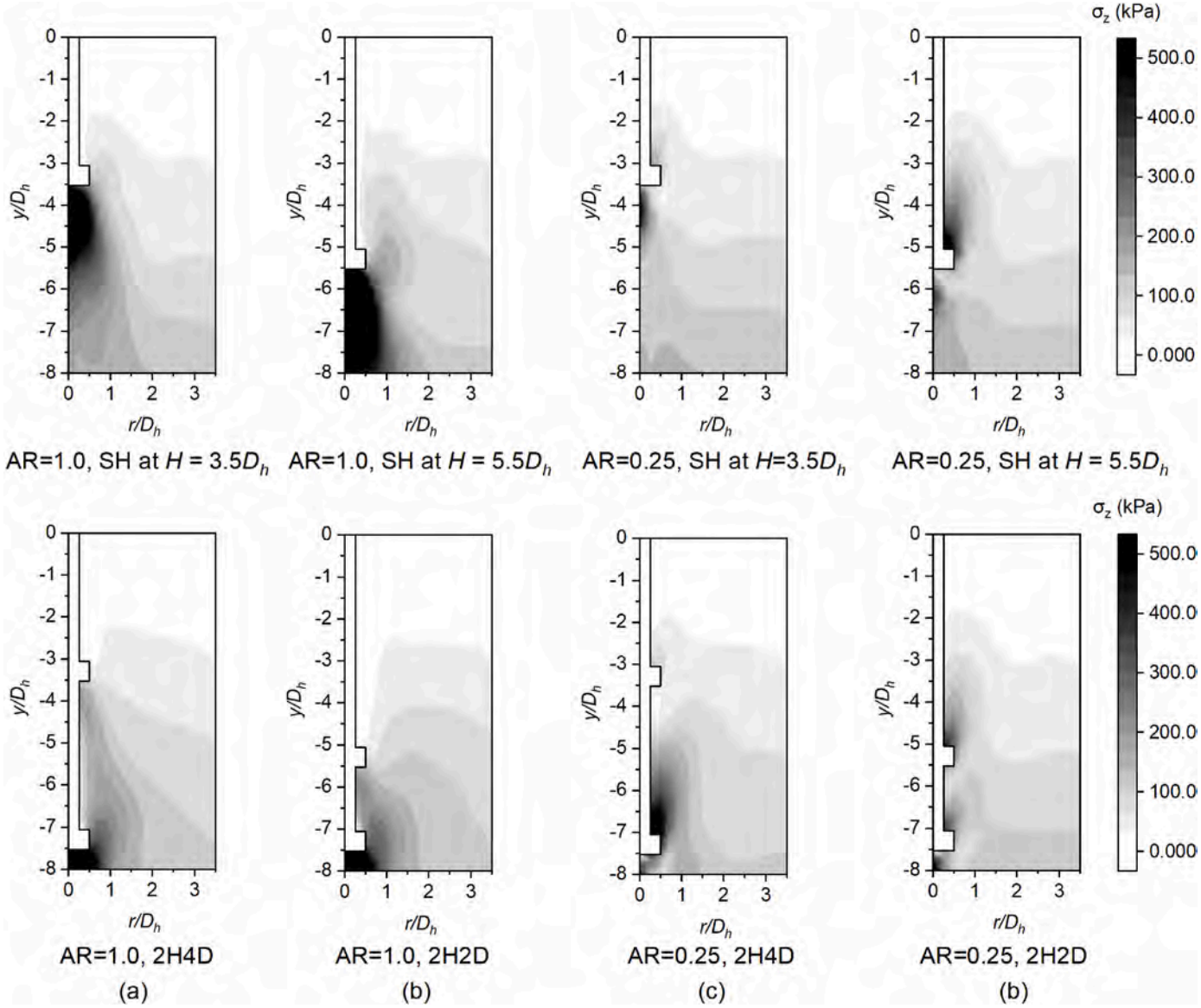

Fig. 21. Effect of installation AR on variation of post-installation vertical stress field induced by penetration of one more helix (a) AR = 1.0, SH at H = 3.5 D_h vs 2H4D; (b) AR = 1.0, SH at H = 5.5 D_h vs 2H2D; (c) AR = 0.25, SH at H = 3.5 D_h vs 2H4D; (d) AR = 0.25, SH at H = 5.5 D_h vs 2H2D (the upper helix of the dual-helix pile and the helix of the single-helix pile are at the same depth in each subplot).

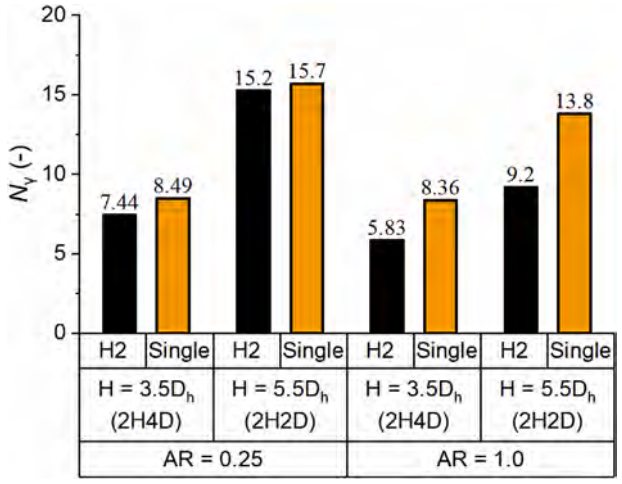

Fig. 22. Effect of installation AR on reduction of helix resistance induced by penetration of an extra helix.

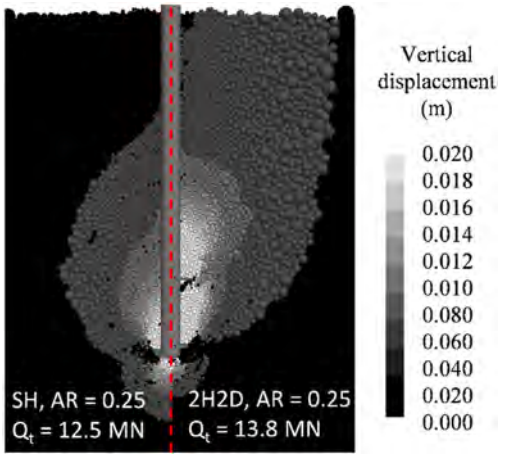

Fig. 23. Tensile failure mechanism and capacity of SH and 2H2D piles at $H_1/D_h = 10.4$ and AR = 0.25 compared at a vertical uplift displacement of $0.1D_h$.

6. Correlation between installation torque and tensile capacity

A capacity – installation torque (K_t, Eq. (1)) is usually used for estimation of screw pile capacity or verification that the installation is as designed. Perko (2009) suggested K_t being a function of shaft diameter D_s:

$$K_t = 1.433/D_s^{0.92} \quad (10)$$

where T is torque at the end of installation.

Fig. 24 shows K_t ranging 2 to 8 for the piles simulated here which is consistent with the findings of Sharif et al. (2021a) who found that K_t varied with installation approach (AR) for the SH pile (amongst other things). It is also notable for the SH, AR = 0.25 case that the results tend to those of Perko (2009) with increasing embedment depth which would be associated with the formation of a deep failure mechanism as per Figs. 18 and 23. This would seem logical in that most small onshore piles typically have low shaft and helix diameters and a relatively high embedment depth ratio which Eq. (10) was derived from. It should also be noted that fundamentally torque correlates with total pile surface area where shaft is the predominant component and capacity predominately correlates with helix diameter and the mechanism developed, in contrast to Eq. (10) where only D_s is considered. Thus, a more reasonable form of Eq. (10) may need to account for the effect of H/D_h and D_h/D_s,

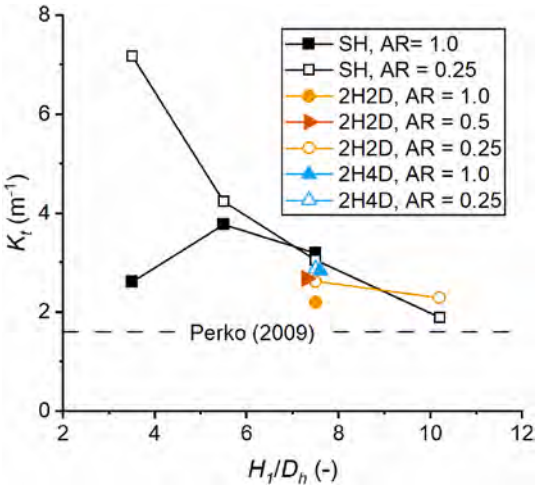

Fig. 24. Summary of tensile capacity – installation torque correlation factor K_t compared to Perko (2009) (data points at $H_1/D_h = 7.5$ may be offset slightly for clarity).

potentially as well as soil relative density as reported by Tsuha and Aoki (2010) and Sharif et al. (2021a)

Furthermore, as discussed previously, the mechanism during installation and tensile loading varies with pile helix number and spacing, installation AR and embedment depth ratio. The value of K_t is related to the complex interaction of those factors and cannot be easily expressed using simple mathematic correlations. For instance, K_t for AR = 0.25 can be either larger or lower than K_t for AR = 1.0 depending on the helix arrangement and installation depth. Therefore, such approaches as using K_t values should be used with caution and not for pile capacity prediction but construction verification as per recommendations in BS8004 (British Standards Institution, 2015).

It is interesting though that for the multi-helix piles that they appear less sensitive to AR and H/D_h and tend to the Perko values. This is surprising based upon the tendency to predominantly shallow mechanisms. This may suggest that the torque of the upper helix during installation is offset by the increased disturbance and reduced relative contribution of the upper helix in uplift and that the Perko (2009) values reflect a lower bound disturbed/mixed capacity and that with better site control (especially of single helix piles) greater capacity contributions could be obtained.

7. Practical implications

Pitch-matched installation, although it is recommended by current standards, may require impractically high vertical force for large-sized offshore screw piles. This installation approach also leads to increased installation torque with helix number. In contrast, over-flighted installation benefits from the reduced vertical force and the potential of decreased torque (up to 26% in this study) resulting from additional helices at a small spacing ($S_h/D_h = 2$).

Using either pitch-matched or over-flighted approaches, it is possible to enhance screw pile tensile capacity by inclusion of an additional (upper) helix when the first (bottom) helix is creating a deep failure mechanism. When the first (bottom) helix tends to develop a shallow failure mechanism, additional helices may be detrimental for tensile capacity. Thus, estimation of critical H/D_h, where shallow/deep failure mechanism transition happens, needs to be built into design and pile configuration when trying to use additional helices to improve pile capacity. For estimation of the critical H/D_h, which is normally based upon soil relative density D_r, the effect of installation AR, i.e. over-flighting increases the critical H/D_h, also needs to be considered.

For optimised tensile capacity, lower helix-spacing may be avoided

even though it may result in a decrease installation torque when over-flighted approaches are adopted. In general a balance between optimised capacity and installation torque needs to be considered if torque is a limitation of the installation equipment.

8. Conclusion

Discrete element modelling was employed to investigate the effect on installation and in-service response of dual-helix screw piles compared to a single-helix pile, with the effects of helix spacing ($S_h/D_h = 2.0$ and 4.0) and advancement ratio being investigated. The piles were installed using pitch-matched (advancement ratio, AR = 1.0) and over-flighted (AR < 1.0, generally 0.25 in this study) approaches, as the latter may be necessary for installation of large size screw piles for offshore applications to minimize excessive vertical push-in forces. The use of DEM revealed the interaction between the two helices during installation, where such insights may not be easily gained from physical modelling or field testing where instrumentation resolution may be relatively low.

Similar to the single helix pile, each helix of the dual-helix piles pushes soil particles downwards and creates relatively high soil stress below itself when installed at AR = 1.0 resulting in large installation compressive force, while when over-flighting each helix moves soil particles upwards and generates high soil stress above the helix resulting in tensile force during installation. The installation torque can also be reduced by adopting lower AR values for a given pile.

The interaction between the two helices during installation is a function of both helix spacing and AR. For installation at AR = 1.0, introduction of an additional (upper) helix leads to higher overall installation vertical force and torque without affecting installation resistance of the first (lower) helix. However, in terms of over-flighting (AR < 1.0), a second helix can displace soil between the two helices upwards again after the first helix passage, resulting in low stress above the first helix if the helix spacing is small (e.g. $S_h/D_h = 2$). As a result, the installation torque measured on the first helix and even the total installation torque is reduced over the single-helix case, in contrast with pitch-matched installation where additional helices typically increase installation force and torque.

The installation induced stress field variation also has effects on in-service tensile response. When installed at AR = 1.0 and $H_1/D_h = 7.5$, the single-helix pile exhibits a deep mechanism. Therefore, an additional helix can improve the overall tensile capacity. While installation at = 0.25 and $H_1/D_h = 7.5$ it tends to create a shallow mechanism for the single-helix pile, resulting in no potential of increased tensile capacity caused by an additional helix and even reduced tensile capacity associated with cylindrical shearing mechanism and decreased stress between the two helices when helix spacing is small. However, this tendency of reduced tensile capacity can be removed by increasing installation depth to a value where a single-helix pile is likely to create a deep failure mechanism. It suggests that it is necessary to consider the deep/shallow mechanism transition induced by adopting different installation AR values when trying to enhance tensile capacity of screw pile by adopting additional helices.

By inspecting the results of both installation requirements and in-service response, it suggests, for screw piles installed using over-flighted approaches, that design of helix spacing needs to consider the balance between tensile capacity and installation torque. Smaller helix spacing can help to reduce installation torque at expense of reduced tensile capacity while larger helix spacing may be needed to maximise tensile capacity although it requires higher torque during installation.

In addition, increasing the number of helices can lead to increased disturbance of the soil and reduced tensile resistance of a helix positioned such that a single depth sees passage of more than one helix. The soil disturbance induced by increased helix number can be reduced by using an over-flighted installation approach. This effect needs to be considered when estimating in-service response of upper helices.

CRediT authorship contribution statement

Wei Wang: Writing – original draft, Software, Conceptualization. **Michael John Brown:** Writing – review & editing, Supervision, Resources, Conceptualization. **Matteo Oryem Ciantia:** Writing – review & editing, Supervision, Resources. **Marco Previtali:** Writing – review & editing, Software. **Yaseen Umar Sharif:** Writing – review & editing, Software. **Craig Davidson:** Writing – review & editing, Investigation.

Declaration of competing interest

The authors declare that they have no known competing financial interests or personal relationships that could have appeared to influence the work reported in this paper.

Acknowledgements

The first author would like to acknowledge the financial support from China Scholarship Council (CSC) and the University of Dundee.

References

Al-Baghdadi, T., 2018. Screw Piles as Offshore Foundations: Numerical and Physical Modelling. University of Dundee, UK. Ph.D Thesis.
Al-Defae, A.H., Caucis, K., Knappett, J.A., 2013. Aftershocks and the whole-life seismic performance of granular slopes. Geotechnique 63 (14), 1230–1244.
Arroyo, M., Butlanska, J., Gens, A., Calvetti, F., Jamiolkowski, M., 2011. Cone penetration tests in a virtual calibration chamber. Geotechnique 61 (6), 525–531.
Bradshaw, A., Zuelke, R., Hilderbranndt, L., Robertson, T., Mandujano, R., 2019. Physical modelling of a helical pile installed in sand under constant crowd. In: Davidson, C., Brown, M.J., Knappett, J., Brennan, A.J. (Eds.), Proceedings of 1st International Symposium on Screw Piles for Energy Applications. University of Dundee, Dundee, UK, pp. 109–115. Dundee, UK, 27-28 May, 2019.
British Standards Institution, 2015. BS8004: Code of Practice for Foundations. BSI, London, UK.
Butlanska, J., Arroyo, M., Gens, A., 2010. Virtual calibration chamber CPT tests on Ticino sand. In: Proceedings of 2nd International Symposium on Cone Penetration Testing, Huntington Beach. California.
Cerato, A.B., Victor, R., 2014. Effects of helical anchor geometry on long-term performance of small wind tower foundations subject to dynamic loads. DFI J. J. Deep Found. Inst. 2 (1), 30–41.
Cerfontaine, B., Brown, M.J., Davidson, C., Sharif, Y.U., Huisman, M., Ottolini, M., 2022. Optimised screw pile design for offshore jacket foundations in medium–dense sand. Géotech. Lett. 12 (2), 114–119.
Cerfontaine, B., Brown, M.J., Knappett, J.A., Davidson, C., Sharif, Y.U., Huisman, M., Ottolini, M., Ball, J.D., 2023a. Control of screw pile installation to optimise performance for offshore energy applications. Geotechnique 73 (3), 234–249.
Ciantia, M., O'Sullivan, C., Jardine, J.R., 2019. Pile penetration in crushable soils: insights from micromechanical modelling. In: H, S., S, E., B, B. (Eds.), Proceedings of 17th European Conference on Soil Mechanics and Geotechnical Engineering. Reykjavik, Iceland.
Cerfontaine, B., Ciantia, M.O., Brown, M.J., Sharif, Y.U., 2021. DEM study of particle scale and penetration rate on the installation mechanisms of screw piles in sand. Comput. Geotech. 139.
Cerfontaine, B., Ciantia, M.O., Brown, M.J., White, D.J., Sharif, Y.U., 2023b. DEM study of particle scale effect on plain and rotary jacked pile behaviour in granular materials. Comput. Geotech. 161.
Cerfontaine, B., Knappett, J.A., Brown, M.J., Bradshaw, A.S., 2019. Effect of soil deformability on the failure mechanism of shallow plate or screw anchors in sand. Comput. Geotech. 109, 34–45.
Cerfontaine, B., White, D., Kwa, K., Gourvenec, S., Knappett, J., Brown, M., 2023c. Anchor geotechnics for floating offshore wind: current technologies and future innovations. Ocean Engineering 279.
Ciantia, M.O., Arroyo, M., Butlanska, J., Gens, A., 2016. DEM modelling of cone penetration tests in a double-porosity crushable granular material. Comput. Geotech. 73, 109–127.
Ciantia, M.O., Boschi, K., Shire, T., Emam, S., 2018. Numerical techniques for fast generation of large discrete-element models. Proceedings of the Institution of Civil Engineers - Engineering and Computational Mechanics 171 (4), 147–161.
Coetzee, C.J., 2017. Review: calibration of the discrete element method. Powder Technol. 310, 104–142.
da Cruz, F., Emam, S., Prochnow, M., Roux, J.N., Chevoir, F., 2005. Rheophysics of dense granular materials: discrete simulation of plane shear flows. Phys. Rev. 72 (2).
Das, B., Shukla, S.K., 2013. Earth Anchors. J. Ross Publishing, Florida, USA.
Davidson, C., Brown, M., Cerfontaine, B., Al-Baghdadi, T., Knappett, J., Brennan, A.J., Augarde, C., Coombs, W.M., Wang, L., Blake, A., Richards, D., Ball, J., 2022. Physical modelling to demonstrate the feasibility of screw piles for offshore jacket-supported wind energy structures. Geotechnique 72 (2), 108–126.

Ding, H., Wang, L., Zhang, P., Liang, Y., Tian, Y., Qi, X., 2019. The recycling torque of a single-plate helical pile for offshore wind turbines in dense sand. Appl. Sci. 9 (19).
Feng, S.J., Fu, W.D., Chen, H.X., Li, H.X., Xie, Y.L., Lv, S.F., Li, J., 2020. Field tests of micro screw anchor piles under different loading conditions at three soil sites. Bull. Eng. Geol. Environ. 80 (1), 127–144.
Galindo, P., Davidson, C., Brown, M., 2018. Installation behavior of open ended and closed ended piles with torque application. In: Proceedings of 1st International Conference on Press-In Engineering, Kochi, Japan. International Press-in Association, pp. 379–386.
Ghaly, A., Hanna, A., Hanna, M., 1991. Uplift behavior of screw anchors in sand. I: dry sand. Journal of Geotechnical Engineering-ASCE 117 (5), 773–793.
Ghazavi, M., Ghomi, Y., Heidari, P., Jelogir, B.M., 2022. Effects of helix shapes and locations on compression capacity of helical piles for offshore foundations. Mar. Georesour. Geotechnol. 41 (6), 634–647.
Giampa, J.R., Bradshaw, A.S., Schneider, J.A., 2017. Influence of dilation angle on drained shallow circular anchor uplift capacity. Int. J. GeoMech. 17 (2).
Herbert-Read, J.E., Kremer, L., Bruintjes, R., Radford, A.N., Ioannou, C.C., 2017. Anthropogenic noise pollution from pile-driving disrupts the structure and dynamics of fish shoals. Proc. Biol. Sci. 284 (1863).
Itasca, 2023. *PFC – Particle Flow Code, Ver. 7.0*, Minneapolis, USA.
Janda, A., Ooi, J.Y., 2016. DEM modeling of cone penetration and unconfined compression in cohesive solids. Powder Technol. 293, 60–68.
Khosravi, A., Martinez, A., DeJong, J.T., 2020. Discrete element model (DEM) simulations of cone penetration test (CPT) measurements and soil classification. Can. Geotech. J. 57 (9), 1369–1387.
Kozicki, J., Tejchman, J., Mróz, Z., 2012. Effect of grain roughness on strength, volume changes, elastic and dissipated energies during quasi-static homogeneous triaxial compression using DEM. Granul. Matter 14 (4), 457–468.
Lauder, K., 2010. The Performance of Pipeline Ploughs. University of Dundee, UK. Ph.D Thesis.
Li, Z., Haigh, S.K., Bolton, M.D., 2010. Centrifuge modelling of mono-pile under cyclic lateral loads. In: Springman, S., Laue, J., Seward, L. (Eds.), Proceedings of Physical Modelling in Geotechnics - Proceedings of the 7th International Conference on Physical Modelling in Geotechnics (ICPMG 2010), vol. 2. CRC Press, Zurich, Switzerland, pp. 965–970, 28th June - 1st July.
Lu, Q., Randolph, M.F., Hu, Y., Bugarski, I.C., 2004. A numerical study of cone penetration in clay. Geotechnique 54 (4), 257–267.
Lutenegger, A.J., 2011. Behavior of multi-helix screw anchors in sand. In: Proceedings of 14th Pan-American Conference on Soil Mechanics and Geotechnical Engineering, Toronto, Ontario, Canada, October 2-6. Canadian Geotechnical Society.
Lutenegger, A.J., Erikson, J., Williams, N., 2014. Evaluating installation disturbance of helical anchors in clay from field vane tests. In: Proceedings of Proceedings of the 39th Annual Deep Foundations Institute Annual Meeting. the US, Atlanta, pp. 21–24. Oct.
McDowell, G.R., Falagush, O., Yu, H.S., 2012. A particle refinement method for simulating DEM of cone penetration testing in granular materials. Géotech. Lett. 2 (3), 141–147.
Meyerhof, G.G., Adams, J.I., 1968. The ultimate uplift capacity of foundations. Can. Geotech. J. 5 (4).
Mitsch, M.P., Clemence, S.P., 1985. The uplift capacity of helix anchors in sand. In: Proceedings of Uplift Behavior of Anchor Foundations in Soil. American Society of Civil Engineers, New York, USA.
Peng, Y., Yin, Z.-Y., 2023. Micromechanical analysis of suction pile-granular soil interaction under inclined pulling load of mooring line: mooring depth effect. Mar. Struct. 92.
Perko, H., 2009. Helical Piles A Practical Guide to Design and Installation. John Wiley & Sons, New Jersey, US.
Rorato, R., Arroyo, M., Gens, A., Andò, E., Viggiani, G., 2021. Image-based calibration of rolling resistance in discrete element models of sand. Comput. Geotech. 131.
Rycroft, C.H., Kamrin, K., Bazant, M.Z., 2009. Assessing continuum postulates in simulations of granular flow. J. Mech. Phys. Solid. 57 (5), 828–839.
Schiavon, A.J., 2016. Behaviour of Helical Anchors Subjected to Cyclic Loadings. Universidade de São Paulo, Brazil. Ph.D Thesis.
Schiavon, J.A., Tsuha, C.d.H.C., Thorel, L., 2019. Monotonic, cyclic and post-cyclic performances of single-helix anchor in residual soil of sandstone. J. Rock Mech. Geotech. Eng. 11 (4), 824–836.
Sharif, Y., Ciantia, M., Brown, M.J., Knappett, J.A., Ball, J.D., 2019. Numerical techniques for the fast generation of samples using the particle refinement method. In: Proceedings of 8th International Conference on Discrete Element Methods, Twente, the Netherland, 21-26 July, 2019. University of Twente, pp. 181–190.
Sharif, Y.U., Brown, M.J., Cerfontaine, B., Davidson, C., Ciantia, M.O., Knappett, J.A., Ball, J.D., Brennan, A., Augarde, C., Coombs, W., Blake, A., Richards, D., White, D., Huisman, M., Ottolini, M., 2021a. Effects of screw pile installation on installation requirements and in-service performance using the discrete element method. Can. Geotech. J. 58 (9), 1334–1350.
Sharif, Y.U., Brown, M.J., Ciantia, M.O., Cerfontaine, B., Davidson, C., Knappett, J., Meijer, G.J., Ball, J., 2021b. Using discrete element method (DEM) to create a cone penetration test (CPT)-basedmethod to estimate the installation requirements of rotary-installed piles in sand. Can. Geotech. J. 58 (7), 919–935.
Sharif, Y.U., Brown, M.J., Ciantia, M.O., Cerfontaine, B., Davidson, C., Knappett, J.A., Ball, J., 2021c. Assessing single-helix screw pile geometry on offshore installation and axial capacity. Proceedings of the Institution of Civil Engineers - Geotechnical Engineering 174 (5), 512–529.
Sharif, Y.U., Brown, M.J., Ciantia, M.O., Lutenegger, A.J., Pavan Kumar, P.V., Patra, S., Haldar, S., 2021d. Using discrete-element method hindcasting of screw pile performance for practical design. Géotech. Lett. 11 (4), 333–339.
Spagnoli, G., Tsuha, C., 2020. A review on the behavior of helical piles as a potential offshore foundation system. Mar. Georesour. Geotechnol. 38 (9), 1013–1036.
Theuerkauf, J., Witt, P., Schwesig, D., 2006. Analysis of particle porosity distribution in fixed beds using the discrete element method. Powder Technol. 165 (2), 92–99.
Tsuha, C.d.H.C., Aoki, N., 2010. Relationship between installation torque and uplift capacity of deep helical piles in sand. Can. Geotech. J. 47 (6), 635–647.
Tsuha, C.H.C., Aoki, N., Rault, G., Thorel, L., Garnier, J., 2012. Evaluation of the efficiencies of helical anchor plates in sand by centrifuge model tests. Can. Geotech. J. 49 (9), 1102–1114.
Ullah, S.N., O'Loughlin, C., Hu, Y., Hou, L.F., 2023. Torsional installation and vertical tensile capacity of helical piles in clay. Geotechnique 1–17.
Wang, D., Merifield, R.S., Gaudin, C., 2013. Uplift behaviour of helical anchors in clay. Can. Geotech. J. 50 (6), 575–584.
Wang, W., Brown, M.J., Ciantia, M.O., Sharif, Y.U., Cerfontaine, B., 2023a. DEM analysis of helix number effects on offshore screw pile installation and in-service performance. In: Zdravković, L., Konte, S., Taborda, D.M.G., Tsiampousi, A. (Eds.), Proceedings of 10th European Conference on Numerical Methods in Geotechnical Engineering. London, UK, June 26 - 28.
Wang, W., Brown, M.J., Sharif, Y.U., Davidson, C., 2023b. The influence of the installation advancement ratio on the cyclic performance of a single-helix pile for floating offshore wind applications. In: Proceedings of 9th International SUT OSIG Conference - Innovative Geotechnologies for Energy Transition. Society for Underwater Technology, London, UK, pp. 1218–1224. September, 12-14.

Glossary

AR: advancement ratio
D_h*:* pile helix diameter
D_r*:* soil relative density
D_s*:* pile shaft or core diameter
d_z*:* uplift displacement of a screw pile during tensile loading
d_{50}*:* mean soil particle diameter
H_n*:* embedment depth of the nth (from pile tip to head) helix
I: system inertial number during screw pile installation
K*:* coefficient of lateral earth pressure
L*:* pile length
L_{pv}, $L_{p\omega}$*:* representative dimension of the plastic deformation zone associated with the vertical rotation and vertical displacement of the helix
N_γ*:* dimensionless factor of helix tensile resistance
n: helix number of a screw pile
p_t*:* thickness of helical plate
p_0'*:* mean effective stress of soil
Q_t*:* tensile capacity
Q_h*:* tensile capacity of a single helix
Q_{cs}*:* cylindrical shearing resistance
r*:* radial distance to the pile centre
SF: scaling factor of particle size
S_h*:* spacing between two adjacent helices
s: ratio of helix spacing S_h to helix diameter D_h
v*:* vertical velocity of screw pile installation
w_h*:* effective width of a helix
y*:* vertical distance to the ground surface
z*:* penetration depth during installation
$\dot{\gamma}$*:* shear strain rate
ρ*:* particle density
σ_r'*:* effective radial stress of soil
σ_v'*:* effective vertical stress of soil
ω*:* rotation rate of screw pile installation